A SOLENOID-BASED ACTIVE HYDRAULIC ENGINE MOUNT: MODELLING, ANALYSIS, AND VERIFICATION

by

Ali Masih Hosseini
B.Sc. of Aerospace Engineering, Sharif University of Technology, 2005
M.Sc. of Biomedical Engineering, RWTH Aachen University, 2008

THESIS SUBMITTED IN PARTIAL FULFILLMENT OF
THE REQUIREMENTS FOR THE DEGREE OF

MASTER OF APPLIED SCIENCE

School
of
Engineering Science,
Mechatronic Systems Engineering

SIMON FRASER UNIVERSITY

Fall 2010

APPROVAL

Name: **Ali Masih Hosseini**

Degree: **Master of Applied Science**

Title of Thesis: **A Solenoid-Based Active Hydraulic Engine Mount: Modelling, Analysis, and Verification**

Examining Committee:

Chair: **Dr. Behraad Bahreyni, P.Eng.**
Assistant Professor of Engineering Science

_____

Dr. Farid Golnaraghi, P.Eng.
Senior Supervisor
Professor of Engineering Science

_____

Dr. Siamak Arzanpour, P.Eng.
Co-Supervisor
Assistant Professor of Engineering Science

_____

Dr. Ash Parameswaran, P.Eng.
Co-Supervisor
Professor of Engineering Science

_____

Dr. Carlo Menon, P.Eng.
Internal Examiner
Assistant Professor of Engineering Science

Date Defended/Approved: November 23 2010

Declaration of
Partial Copyright Licence

ABSTRACT

The focus of this thesis is on the design, modelling, identification, simulation, and experimental verification of a low-cost solenoid-based active hydraulic engine mount. To build an active engine mount, a commercial On-Off solenoid is modified to be used as an actuator and it is embedded inside a hydraulic engine mount. The hydraulic engine mount is modelled and tested, solenoid actuator is modelled and identified, and finally the models were integrated to obtain the analytical model of the active hydraulic mount. Then the active mount is tested and showed that the analytical model can closely predict its behaviour.

In future, the developed model can be used for designing the vibration control system of this active mount. This active mount can potentially work as part of an active noise and vibration control (ANVC) system in automotive or other closely related applications as an alternative to more expensive active mount systems.

Keywords: Solenoid modelling, Active hydraulic engine mount, Lump model, Linear system modelling, Parameter identification.

To memory of Ali Rouhani

ACKNOWLEDGEMENTS

I started this project on July 2009 and defended it on November 2010. I suffered from a neck injury last March that had huge physical and emotional impact on me. I made many sacrifices during this period; this project would not be done without my perseverance and commitment.

I would like to mention and express my gratitude to Farid Golnaraghi, my senior supervisor, who offered me the great opportunity to work as his graduate student. His offer literally changed my life. I would like to thank my co-supervisor, Siamak Arzanpour; his advices on research direction, practical tests, and the final manuscript, were substantial and absolutely invaluable. I highly appreciate my co-supervisor, Ash Parameswaran, for reviewing my works and supporting me financially along my other supervisors though AUTO21. I thank Carlo Menon, my examiner, for accepting to read and evaluate this thesis. I also thank our helpful office staffs, Jennifer Leone, Kinga Muntener and Julibeth Fernandez as well as our laboratory and machine shop staffs, Taha Al-Khudairi and Mustafa Sajid.

Thanks to Esmaeil Tafazzoli, Hossein Mansour, Kaveh Kianfar, Hadi Esmaeilsabzali, Amr Marzouk, Neda Parnian, Parvind Grewal, and Mahdi Alavi for the discussions on the technical material. I thank my mom, Farideh Rouhani, my dad, Hassan Hosseini, and my sisters Maha and Mahsa for their all-time support and love; I am blessed and proud to have such a family.

This past two years at SFU was a great life experience for me; I learnt important life lessons to carry with me forever. Cheers!

Masih, November 2010

Vancouver, B.C.

TABLE OF CONTENTS

LIST OF FIGURES

LIST OF TABLES

NOMENCLATURE

A_r = Effective piston area of the rubber [mm^2]
A_e = Effective area of the solenoid core perpendicular to the magnetic flux [mm^2]
A_s = Effective pumping area of the plunger [mm^2]
A_i = Effective area of the inertia track [mm^2]
B_r = Damping of rubber [N.s/mm]
B = True damping of the hydraulic mount [N.s/mm]
$B(\omega)$ = Frequency dependant, true damping of the hydraulic mount [N.s/mm]
b_s = Damping of plunger [N.s/mm]
b = Damping [N.s/mm]
b_i = Damping of water-mass in the inertia track [N.s/mm]
$C_{1,2}$ = Compliance of the upper chamber, lower chamber [mm^5/N]
$C_{\overline{F_T X_e}}$ = Passive coefficient of the dynamic stiffness [N/mm]
$C_{\overline{F_T I_s}}$ = Active coefficient of the Transmitted force [N/A]
F_T = Force transmitted [N]
F_s = Solenoid force applied to plunger [N]
$\widehat{F_s}$ = Approximate force of the Solenoid [N]
$F_{T_{sol}}$ = Force transmitted, solenoid's contribution [N]
F_1 = Force on the top of the water-mass of inertia track [N]
F_2 = Force on the bottom of the water-mass of inertia track [N]
f = Pre-compression force [N]
G_s = Solenoid's force gain [N/A]
H_c = Magnetic field intensity in core [AT/mm]
H_g = Magnetic intensity in air-gap [AT/mm]
H_p = Magnetic intensity in plunger [AT/mm]
I_i = Fluid inertia of the inertia track [N/mm^5]
I_s, I, i_s = current to the coil [A]
k_1 = Apparent stiffness of the upper chamber's compliance [N/mm]
k_2 = Apparent stiffness of the lower chamber's compliance [N/mm]
k_s= Plunger stiffness [N/mm]
$K_{dyn|_{pass}}$.= Dynamic stiffness of passive mount [N/mm]
$K_{dyn|_{act}}$.= Dynamic stiffness of the active mount [N/mm]
K_r = Stiffness of rubber [N/mm]
K = Pure stiffness of hydraulic mount [N/mm]
$K(\omega)$ = Frequency dependant stiffness of hydraulic mount [N/mm]
L = Magnetizing inductance of the coil [s.Ω]
l_c = Effective length of magnetic flux in core [mm]
l_p = Effective length of magnetic flux in the plunger [mm]
l_g = Effective length of the air-gap [mm]

M_i = Mass of water in inertia track [Kg]
M_e = Mass of engine [Kg]
N = Number of coil turns
$P_{1,2}$ = Pressure of the upper and lower chambers respectively [N/mm^2]
Q_i, q_i = Flow rate in the inertia track [mm^3/s]
$r = \omega_b/\omega_n$ = Frequency ratio
R_i = Inertia track resistance [N-s/mm^5]
$\Re_p$= Reluctance of plunger [1/H]
$\Re_c$= Reluctance of core [1/H]
$\Re_a$= Reluctance of air-gap [1/H]
s = Laplace transform variable
T_r = Transmissibility
t = time [s]
W_m = Magnetic field energy [Jouls]
X_e, x_e = Engine displacement [mm]
x_0 = Soelnoid's initial air-gap [mm]
x_s = Plunger displacement [mm]
X/Y = Displacement transmissibility ratio
$\omega_n = \sqrt{k_s/m_s}$ Natural frequency of plunger [rad/s] or [Hz]
ω_b = Frequency of base excitation [rad/s] or [Hz]

ω = frequency of oscillation [rad/s] or [Hz]
$\omega_1 = \sqrt{\frac{1}{I_i C_2}}$ = Switching frequency of dynamics stiffness (low freq.) [rad/s] or [Hz]
$\omega_2 = \sqrt{\frac{1}{I_i C_1}}$ = Switching frequency of dynamics stiffness (high freq.) [rad/s] or [Hz]
Φ_k = Dynamic stiffness phase [Deg.]
ϕ = Magnetic flux [volt.s]
μ_0 = Permeability of free space [H-mm^{-1}]
μ_p = Permeability of plunger [H-mm^{-1}]
μ_c = Permeability of core [H-mm^{-1}]
ζ = Damping coefficient
ζ_{T_r} = Coefficient of transmissibility reduction
ζ_k = Coefficient of dynamic stiffness tuning

Chapter 1: INTRODUCTION

1.1 Engine Mounting

In road vehicles, the cabin noise, vibration, and harshness (NVH) is an important indicator of ride quality and passenger comfort; NVH relates directly to the chassis condition. Two major sources of forcing on the chassis are engine vibration and road-induced vibration. The suspension system relates to the issue of the road-induced vibration, whereas the engine mounting relates to engine-induced vibration. The huge power generated by the engine must transfer smoothly to the wheels without rattling the vehicle too much or twisting the engine as a result of the generated torques on the crankshaft. The engine must be kept tightly in place and not move excessively due to the inertial loadings (e.g. turns) or the road inputs (e.g. road bumps).

An engine mount is a vehicle component that attaches the engine bracket to the chassis. The engine is connected to the car's body by several mounts, which are important for smooth operation of the vehicle. An engine mount should isolate the passengers' cabin from engine-generated noise and vibration. The engine mount must also hold the engine in place and restrict it from moving.

Engine vibrations have two major sources: (1) intermittent pulsing due to ignition in the engine cylinders, and (2) inherent unbalances in the reciprocating components of the engine. The frequency of the vibration depends on the number of cylinders, stroke number, and engine speed. For example, in a four-stroke engine, the frequency of fundamental ignition disturbances is at the second order of engine speed. Therefore, for a four-cylinder engine in speed range of 600-6000 rpm, the frequency range of disturbances is 20-200 Hz. For a four-stroke, eight-cylinder engine,

the frequency range is 40-400 Hz over the same engine speed range. On the other hand, the frequency of the fundamental engine unbalance disturbances is the same as the engine speed. So that, for a four-cylinder engine in speed range of 600-6000 rpm, the frequency range of fundamental unbalance disturbances is 10-100 Hz.

Connection of the engine to the chassis, in mechanical element terms, can be simplified as a mass (the engine) connected to the chassis via a parallel damping and stiffness element (Figure 1-1). So the transmitted force from engine vibration to the chassis is related to the damping and stiffness of the mount.

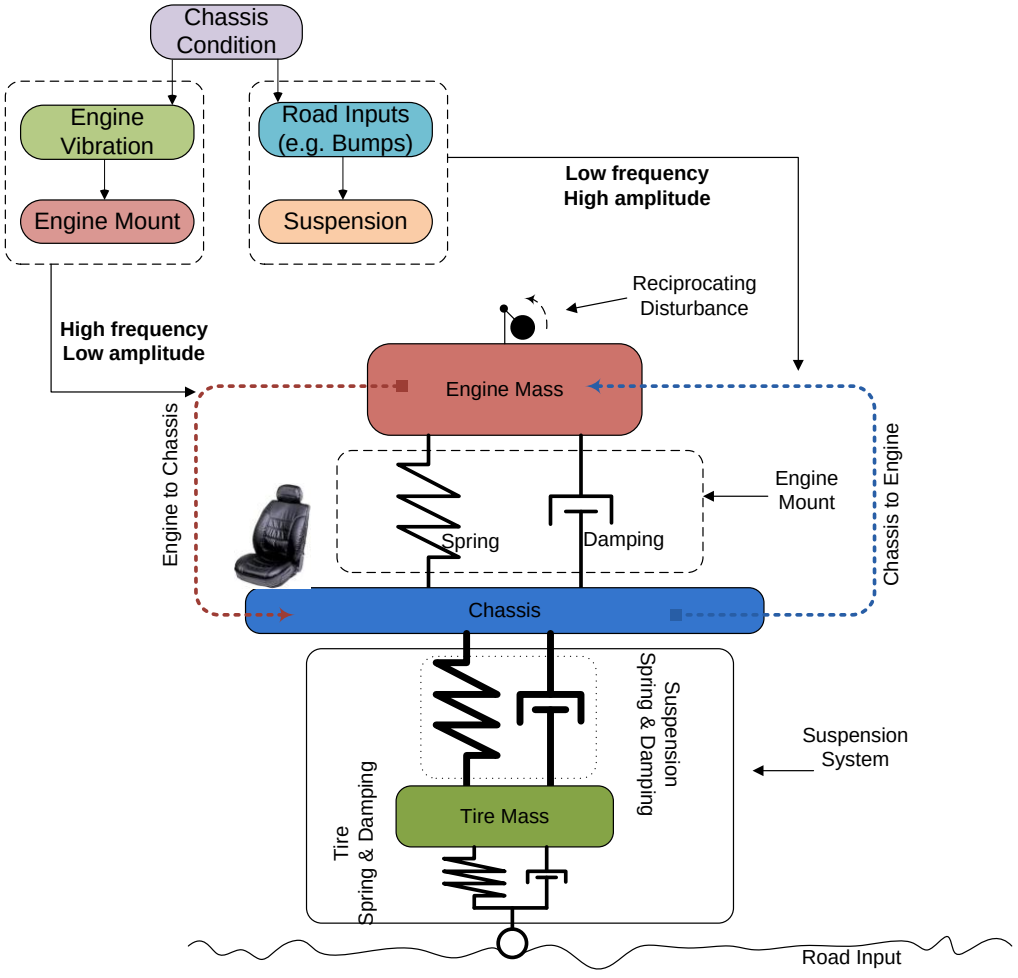

Figure 1-1: Engine and road disturbances pathway to the chassis in a simplified quarter car lumped model.

An engine mount (1) prevents an engine from harsh movements, (2) supports the weight of the engine, and (3) isolates chassis from engine vibration forces. The behaviour of an engine mount is usually reported in terms of its frequency response for different amplitude excitations. Frequency/amplitude ranges of greatest interest include [**1**]: (1) low-frequency high-amplitude 5-15 Hz, 0.5-5 mm—these excitations are in the range of engine resonance and large enough to require significant damping; (2) high-frequency low-amplitude 25-250 Hz, 0.05-0.5 mm—these excitations can cause noise and vibration, and require good isolation.

Taking a look back at Figure 1-1, we can see that the vibration of the chassis and engine mount can be simplified as a base excitation problem (See Figure 1-2). In Figure 1-2, the mass m is excited by harmonic motions of base [**2**].

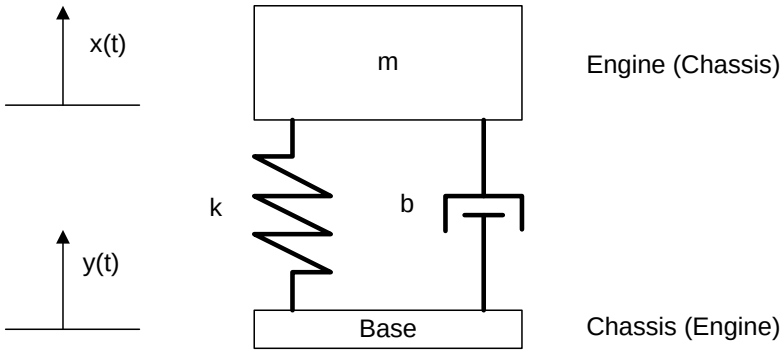

Figure 1-2: Base excitation problem models the motion of an object of mass being excited by prescribed harmonic displacement acting through the spring and damper.

Summing the relevant forces on the mass, Figure 1-2 yields:

$$m\,\ddot{x} + b(\dot{x} - \dot{y}) + k(x - y) = 0\,. \tag{1.1}$$

For the base excitation problem it is assumed that the base moves harmonically, that is, that

$$y(t) = Y sin\ \omega_b t, \tag{1.2}$$

where Y denotes the amplitude of the base motion and ω_b represents the frequency of the base oscillation. Substitution of $y(t)$ from previous equation in (1.1) yields, after some rearrangement,

$$m\,\ddot{x} + b\dot{x} + kx = bY\omega_b\, cos\ \omega_b t + kY sin\ \omega_b t\,. \tag{1.3}$$

Dividing equation (1.3) by m and using the definitions of damping ratio and natural frequency yields

$$\ddot{x} + 2\zeta\omega_n\dot{x} + \omega_n^2 x = 2\zeta\omega_n\omega_b Y\, cos\ \omega_b t + \omega_n^2 Y sin\ \omega_b t\,. \tag{1.4}$$

After solving the differential equation (1.4) and further rearrangements, the particular solution of (1.4), denoted by X, will be

$$X = Y\left[\frac{1 + (2\zeta r)^2}{(1 - r^2)^2 + (2\zeta r)^2}\right]^{\frac{1}{2}}. \tag{1.5}$$

where r is the frequency ratio $\frac{\omega_b}{\omega_n}$. The details of obtaining the solution can be found in vibration text books such as D.J. Inman [**2**]. $\frac{X}{Y}$ ratio expresses the ratio of the maximum response magnitude to the input displacement magnitude. This ratio is called the displacement transmissibility. This ratio is plotted in Figure 1-3. For design of a proper engine mount, we always want to stay on the lowest displacement transmissibility curve possible.

Note from the figure that for $r < \sqrt{2}$ the transmissibility ratio is greater than 1. Low frequency road and suspension induced chassis motion (here chassis is considered the base) is in

this frequency range (we call this frequency range, the fixture zone). Therefore the chassis motion will be amplified and causes the engine displacement. To avoid excessive displacement of the engine we would like to increase the damping coefficient of the engine mount ζ (the lower displacement transmissibility curve). Also by decreasing the frequency ratio r we can move away from the transmissibility peaks (to the left hand side of the curve) that occur around the resonance frequency $r = \frac{\omega_b}{\omega_n} = 1$. To do that we must increase the stiffness of the mount to obtain an engine mount with a higher natural frequency. So in fixture zone we require high stiffness and high damping.

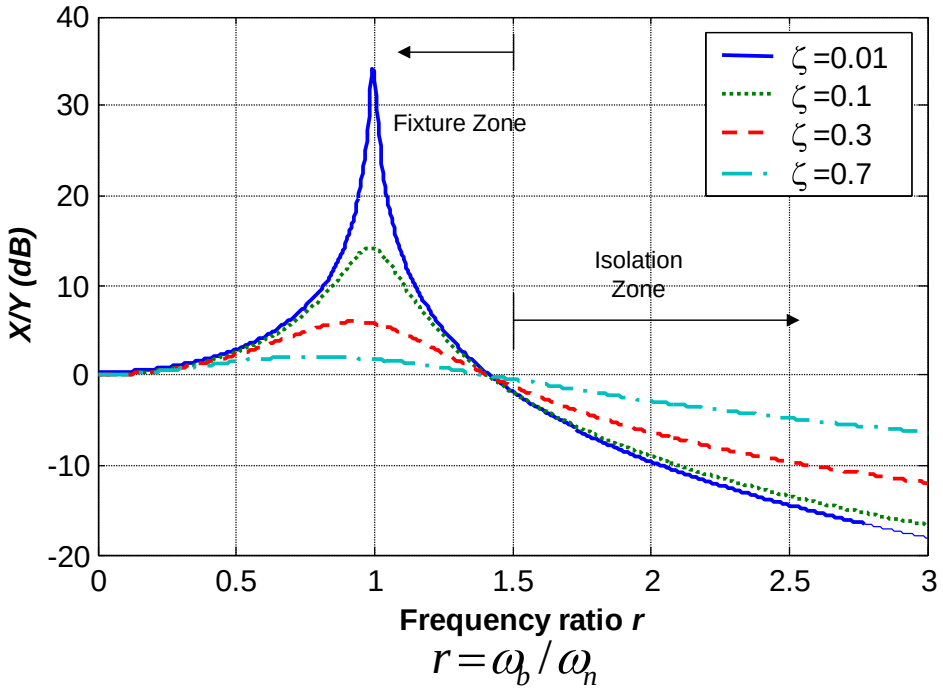

Figure 1-3: Displacement transmissibility as a function of frequency ratio, illustrating how the dimensionless deflection X/Y varies as the frequency of the base motion increases for several different damping ratios.

On the other hand, in higher frequencies (here engine is considered the base) where $r > \sqrt{2}$ the displacement transmissibility ratio is lower than 1 and the motion of the mass is of

smaller amplitude than the amplitude of the exciting base motion (we call this frequency range, the isolation zone). A proper engine mount must minimize the transmissibility ratio (transmissibility from engine into the chassis). Therefore it is desirable that the engine mount have a very low damping in isolation range. Also it is desirable to increase the frequency ratio (further to the right) to lower the displacement transmissibility in this region. To do that, we must decrease the stiffness of the engine mount. So in isolation zone we require low stiffness and low damping.

1.2 Rubber Mount

Different types of engine mounts are used in vehicles. Rubber mounts (or elastomeric mount) are low cost and the simplest type of mounts. A rubber mount consists of a bulk rubber, casted on a metal casing, and a mounting rod. These mounts suppress engine force/torque and vibrations through thermal dissipation.

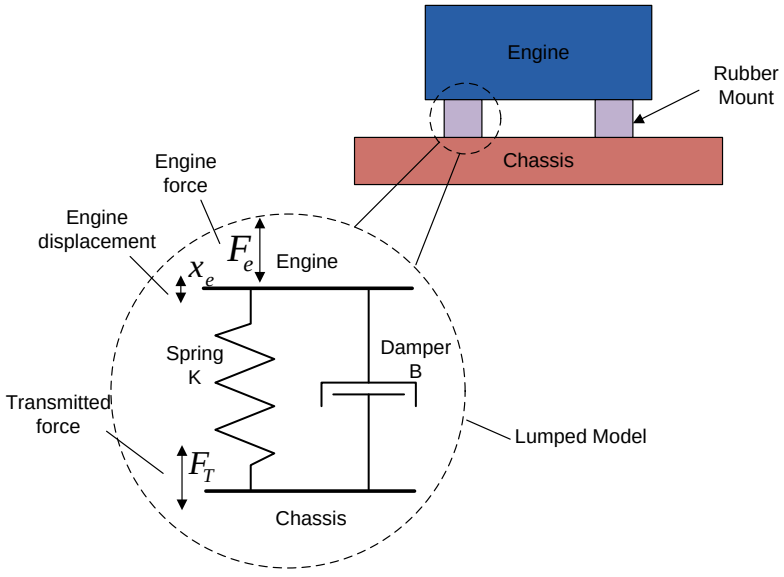

Figure 1-4: Lump model of a rubber mount.

A rubber mount can be simply modelled by a spring damper (Figure 1-4). The transmitted force, F_T, to the chassis in terms of engine vibrations is:

$$F_T = Kx_e + B\dot{x}_e, \tag{1.6}$$

and writing the previous equation in Laplace domain we have:

$$F_T(s) = (K + sB)X_e(s). \tag{1.7}$$

The transmitted force over the engine displacement is called "dynamic stiffness" and it is an indication of hardness of the mount,

$$K_d(s) = \frac{F_T(s)}{X_e(s)}. \tag{1.8}$$

The dynamic stiffness of the rubber mount based on the lumped model is:

$$K_d(i\omega) = K(\omega) + i\omega B(\omega). \tag{1.9}$$

$K(\omega)$ and $\omega B(\omega)$, are stiffness force (real part) and damping force (imaginary part) of the mount respectively, where B is the damping coefficient. For a rubber, we can assume that stiffness K and damping coefficient B are constant. The contribution of damping coefficient in the transmitted force increases linearly by increase of the vibration frequency, and the slope of this increment is damping coefficient B.

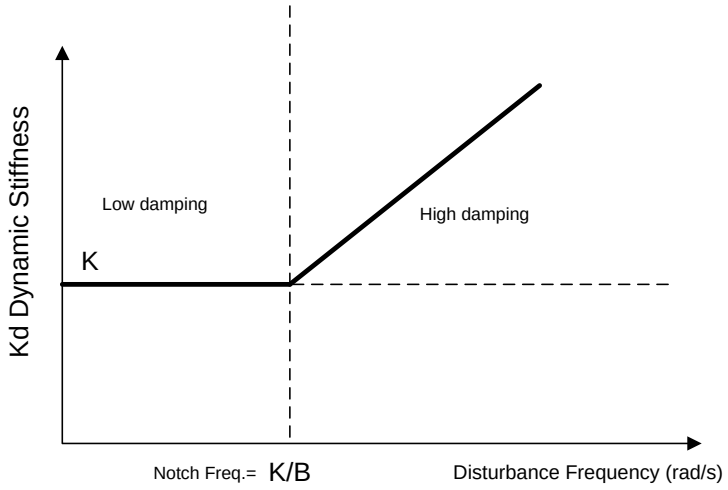

Figure 1-5: Dynamic stiffness of a rubber mount.

A rubber mount can provide the required stiffness for the resonance control and shock absorption, but the rubber damping in low frequencies is not sufficient. Moreover, the isolating characteristic of the rubber mount is not good because the transmitted force increases in higher frequencies due to the constant damping (high stiffness and high damping force in the isolation zone). So that the rubber mount somehow satisfies the fixture zone requirement but cannot address the soft state (low damping low stiffness) requirements in higher frequencies for isolation (Figure 1-5).

1.3 Hydraulic Engine Mount

Hydraulic engine mounts are first patented by Richard Rasmusen in 1962, to improve ride comfort and reducing the NVH in the cabin. Hydraulic mounts are passive engine vibration isolators used for addressing the isolation problem of the rubber mounts that described in the previous section.

A hydraulic mount, depicted in Figure 1-6, has two chambers; (1) main rubber chamber, and (2) compensation chamber, both filled with a mixture of water and ethylene glycol. The

upper chamber (main rubber) exhibits small compliance since it supports most of the static load of the engine and therefore it is manufactured thick. The lower chamber (compensation chamber) is made of thinner rubber and exhibits more compliance therefore it is called compliance chamber. The two chambers are connected by two different fluid passages, (1) decoupler and (2) inertia track. Decoupler is a fluid gate which is activated with a displacement restricted floating plate. Decoupler has an amplitude/frequency dependant characteristic. In high-amplitude-low-frequency vibrations it bottoms out and closes the fluid gate. Whereas, in the low-amplitude-high-frequency region, it is open and remains as a fluid connection path between the two chambers. The inertia track is an annular narrow track in the plate, and it is the other connection route between the two chambers. Since the engine vibrations cause the upper chamber to pump the fluid into the compliance chamber through the two fluid passages, it is called the pumping chamber.

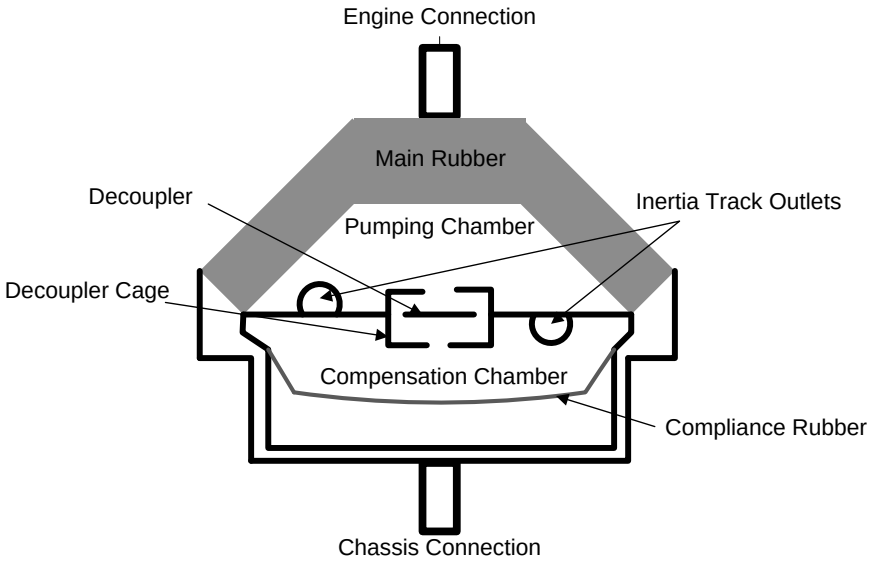

Figure 1-6: Schematic cross section of a hydraulic engine mount.

A hydraulic engine mount has both continuous and discontinuous non-linearities and its parameters vary significantly with the amplitude and frequency of vibrations. Typical non-linear characteristics include the non-linear chamber compliances, vacuum formation in the top chamber during the expansion process, non-linear fluid resistances, and the switching mechanism of the decoupler [**3**].

At low frequencies excitations the decoupler closes because of the high amplitude nature of the excitation. The only fluid connection pathway will be the inertia track. Inertia track has a resistance that damps out the fluid motion through converting it to the heat and through this mechanism it produces damping. At high frequencies excitation where the deflection amplitude is small (less than 0.1 mm) the decoupler plate does not contact with the gate and vibrates at the middle of the gate. So that the decoupler gate stays open and provides a low resistance pathway of fluids. The resistance of the inertia track is much higher than the resistance of the open decoupler gate. Therefore, decoupler gate will be the main fluid connection between the two chambers. This creates frequency dependant dual characteristics in the hydraulic mount: (1) higher energy dissipation in the inertia track in low frequency region (hard state, decoupler closed) and (2) lower energy dissipation in low frequency region (soft state, decoupler open). Figure 1-7 shows the dynamic stiffness of a hydraulic engine mount over a frequency range in response to different amplitude of vibrations. The mount exhibits an amplitude dependant characteristic with hard state in response to high amplitude vibrations (shock and resonance) and soft state in response to the low amplitude vibrations (engine high frequency vibration).

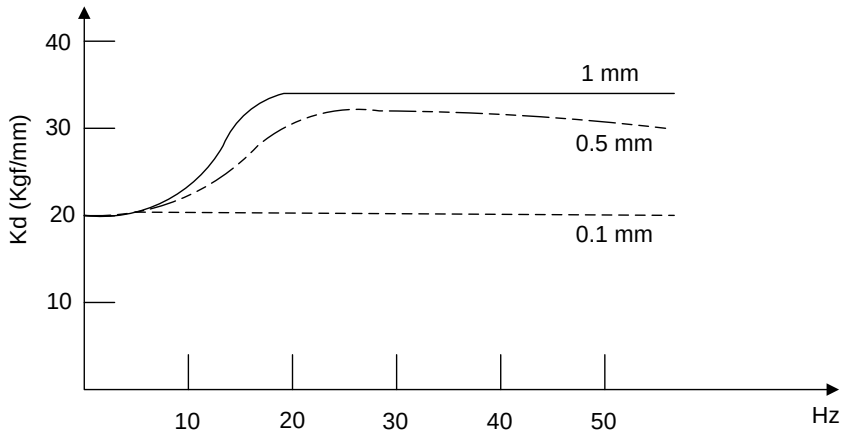

Figure 1-7: Dynamic stiffness of a hydraulic engine mount. (Approximately reproduced from [**4**])

There has been considerable amount of research work carried out by different authors on modelling of the engine mount and comparison between the rubber mount and the hydraulic mount. Generally, a lumped model is used for modelling of the hydraulic engine mount (Figure 1-8).

Singh et. al. [**5**] proposed a linear time invariant (LTI) model for a hydraulic engine mount with lumped mechanical and fluid elements, and validated the model by comparing dynamic stiffness predictions with experimental data over the frequency range 1-50 Hz. Colgate et. al. [**1**] proposed a piecewise linear simulation and an equivalent linearization technique to explain the amplitude dependence of frequency response as well as the composite input response of the mount.

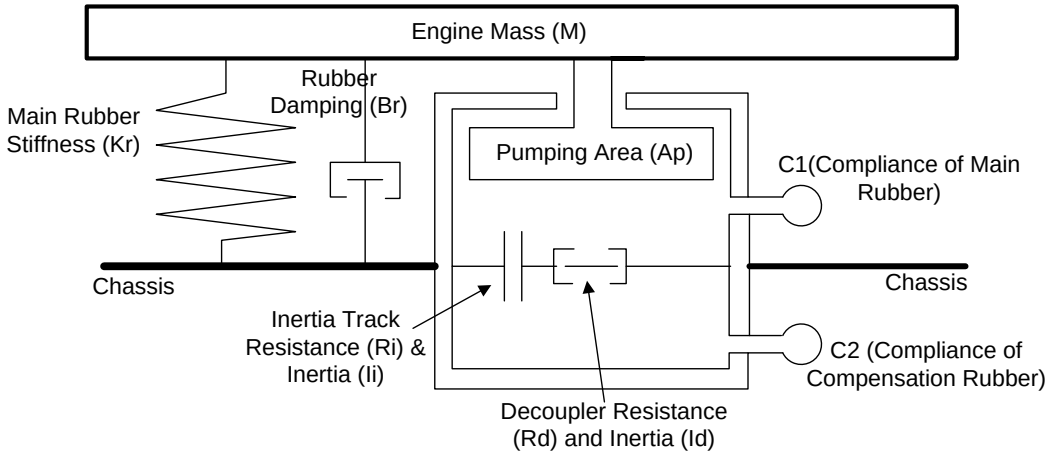

Figure 1-8: Lump model of a hydraulic engine mount.

Geisberger et. al. [**6**] [**7**] developed a complete non-linear model of a hydraulic engine mount and experimentally evaluated the model. The model is capable of capturing both the low frequency and high frequency behavior of the hydraulic mount.

Ohadi and Maghsoodi [**8**] used a multi-DOF engine model in their engine mount studies and simulated a six-degrees-of-freedom, V-shaped, four-cylinder engine and studied the effects of the vibrations of the motor on the hydraulic engine mount and rubber mount. Their study provides a platform for engine mount optimization and sizing.

Problem Description

To increase the MPG of cars, the general trend in the automotive industry is decreasing the weight of the vehicle. This makes the cars more vulnerable to NVH disturbances including engine vibration. Moreover, the engines are becoming more powerful and therefore, the force transmission to the chassis results in even more NVH. The problem is becoming more serious in the case of variable displacement engines (VDE); these engines reduce the fuel consumption and emission by deactivating one or more cylinders or altering the displaced fuel/air volume.

Therefore, the vibration pattern will change based on the engine load and the number of cylinders in action. Passive engine mounts are not flexible enough to switch to different operational modes to cope with the changing vibration pattern. A controllable mount is desirable, because its characteristics can be tuned based on the engine vibration isolation requirements. In the following section we review some of the works carried out in the field of active engine mounts that are in line with our research.

1.4 Active and Semi-Active Engine Mounts

Active and semi-active mounts are introduced to improve the adaptability of dynamic stiffness and performance flexibility of the passive hydraulic mount. Semi-active mounts dissipate energy similar to passive elements, but the resistance of these mounts is adjustable. In contrast to semi-active mounts, the active mounts alter the dynamic performance of engine mounts by applying force through an actuator.

Different types of actuators have been used in engine mount designs. Electro-rheological fluids [**9**] [**10**], magneto-rheological fluids [**11**], and on-off solenoid valves [**12**] [**13**] have been used in semi-active engine mounts. Voice coil [**14**], piezoelectric actuator [**15**], servo-hydraulic actuator [**16**], and electromagnetic inertia-mass [**17**] [**18**], have been used in active engine mount design.

Literature Review of Semi-Active Engine Mounts

Kim and Singh [**13**] developed a new adaptive mount system that exhibits broad bandwidth performance features up to 250 Hz. It implements an on-off damping control mode by using engine intake manifold vacuum and a microprocessor-based solenoid valve controller.

Choi and Choi [**10**] presented feedback control characteristics of a shear-mode-type electro-rheological (ER) engine mount. They measured the field-dependant yield stress of an Arabic gum-based ER fluid using an electroviscometer and incorporated it into the governing equation of the motion of the ER engine mount. Then they designed a sliding mode controller. They found out that their proposed ER engine mount capable of isolating the isolating the sinusoidal and random vibrations.

Choi et. al. [**9**] evaluated the isolation performance of the ER engine mount with different intensity of electric fields in the frequency domain and compared them with that of a conventional hydraulic mount. They derived the governing equations of motion in coupling with engine excitation forces and the full car model. They applied H_∞ control algorithm and evaluated the engine displacement and body acceleration via hardware-in-loop simulation (HILS) at different engine excitation frequencies.

Foumani et. al. [**14**] introduced an adaptive hydraulic engine mount that can be tuned to road and engine conditions by changing the length of the inertia track and effective decoupled area in low-frequency road and high-frequency engine excitations. A single solenoid valve was used to change the inertia track and decoupler area of the mount in both low frequency and high frequency regimes. Sensitivity analysis and numerical studies showed promising results that are superior to passive hydraulic mount.

Ahmadian [**11**] studied the effect of various parameters of a magneto-rheological (MR) mount on the vibration isolation performance of the mount. The mount he used, incorporated MR fluid in a conventional fluid mount to activate and deactivate an inertia track.

Literature Review of Active Engine Mounts

Ushijima [**15**] investigated piezoelectric actuators (PAs) in engine mounts. Piezoelectric actuators have high speed response, but the displacement is generally very small. Therefore, a PA mount requires an amplitude magnifying mechanism, and Ushijima proposed a PA mount with an enlargement mechanism. He also modified the adaptive control algorithm described by S.J. Elliot [**19**], significantly attenuating the dominant harmonics.

Hodgson [**17**], analytically and experimentally, studied the control of active isolators with servo-hydraulic actuators. Fursdon [**14**] proposed an active mount which has an electromagnetic actuator and a self-tuning noise cancellation algorithm. His engine mount is a combination of a passive hydraulic mount with a voice coil actuator. He claims that it generates a force greater than 40 N in a wide range from 25 to 200 Hz. and that the motion of the voice coil changes the pressure in the upper chamber of the hydraulic engine mount to reduce the force on the engine and chassis.

Hillis et. al. [**20**] [**21**] developed adaptive vibration isolation control methods for the active mount developed in [**14**]. The error-driven minimal control synthesis (Er-MSCI) algorithm with integral action has been applied, but the method exhibited gain windup due to actuator saturation. The integral action of the Er-MSCI algorithm was responsive to the high amplitude chassis motions (e.g. going over a bump) and can result in saturation of the actuator. So that they developed a new controller, the narrow-band MCS (NBMCS), intended specifically for narrow-band applications. This way, the frequency of engine disturbance is detected and the NBMCS tries to suppress the force disturbance in the specific narrow target range to avoid receiving feedback from other chassis motions. The frequency of the significant disturbance is detected and controlled. NBMCS is based on Er-MCSI but it benefits from the deterministic nature of the

system disturbance. as the engine disturbance frequency is correlated to the engine RPM and that can be obtained from ECU (engine computing unit). The NBMCS algorithm is shown not to suffer from the gain windup problem. The filtered-x least mean square (FXLMS) algorithm is a popular adaptive feedforward control method, and is widely used in active noise and vibration control applications. Its popularity is due to its relatively simple implementation and well studied convergence behaviour. Hillis et. al. also compared the FXLMS adaptive filter as a benchmark with the Er-MCSI and NBMCS. Er-MCSI had computational advantages over FXLMS because it does not require cancellation path modelling. Their studies showed both of their adaptive control algorithms reduced the accelerations on the chassis by 50-90% under normal driving conditions.

There are commercial active engine mount manufacturers such as Continental AG [**22**] [**23**] and DTR VMS [**24**] [**14**]. There are also vehicles such as Honda Accord 2010, Honda Odyssey 2005, Lexus RX350 2007, Jaguar XJ 2006, Hyundai Veracruz 2007, and Toyota Camry 2007 that have active engine mounts. These shows that the active engine mount technology has made its ways from laboratories into automobile manufacturing industry and highly competitive and successful companies such as Honda is utilizing them in their well-established products. On the other hand the cost is a very important player in this industry. Cutting the cost of an active engine mount without jeopardizing the performance of it can be considered as a breakthrough towards employing the active engine mount system in lower end cars as well as high end luxury cars.

1.5 Thesis Outline

In the first Chapter the need for engine mounting has been declared and then different types of mounts have been introduced (rubber mount, hydraulic mount, semi-active mount, active

mount). State-of-the-art and the literature on design, modelling and control in field of active engine mounts have been reviewed.

In Chapter 2 the governing equations of the hydraulic engine mount is developed using the lumped modelling approach. The concept of dynamic stiffness and mount transmissibility are introduced. The model is then tested and the parameters of the hydraulic mount are extracted using a curve fitting method. After validating the model with the experiments, the extracted parameters are used in further simulation studies and different characteristics of the hydraulic engine mount are predicted. Then based on an industry report on requirements of desirable engine mount characteristics, we discuss that the characteristics of the hydraulic mount does not satisfy the proper engine isolation for all the engine status and drive/road condition. Therefore there is a need for designing a tunable/controllable engine mount to address different engine mount requirements.

In Chapter 3, we present the design of a novel, low-cost, solenoid-based active engine mount. The presumptions behind the design configuration are explained. Then we explained how we made an actuator for vibration control, using an on-off solenoid valve. Then the model of the actuator has been developed using electromagnetic and mechanical equations. The resulting model is highly nonlinear therefore the model is linearized based on realistic assumptions. The static properties of the solenoid such as stiffness, mass, and geometrical sizes are measured. Dynamic frequency response tests are performed on the solenoid actuator. Then the results are matched to our linearized mathematical model of our actuator and the unknown dynamic parameters such as actuator force gain, and the damping of actuator are identified.

In Chapter 4, the mathematical model of actuator is integrated into the engine mount model. Then the whole governing equations of the active engine mount (which is a MIMO

system) is presented in a compact state-space form. Based on an assumption that the system is linear, and the fact that we tested the passive and active parts of the active engine mount model separately (in Chapter 2 and Chapter 3 respectively), we use the developed model of the active engine mount for further simulation studies. The effects of different parameters on the performance of the active engine mount are studied. The tuning of dynamic stiffness and control of transmissibility are discussed after that. Then we experimentally proved that the force output of our active engine mount is in close agreement with the theory. Then we demonstrated that an active engine mount dynamic stiffness control for a real condition that could not be met by the conventional hydraulic engine mount.

Chapter 5 presents the conclusions of the work and recommends the future direction of this research.

Chapter 2: MODELLING OF HYDRAULIC ENGINE MOUNT

In the previous chapter, the rubber mount and hydraulic engine mount have been introduced. The components of a hydraulic engine mount were explained in section 1.3. As mentioned before the static load of the engine is supported by the main rubber of the mount. When the hydraulic mount is subject to dynamic loads (from engine or chassis), the extra mechanical load causes an increase in the fluid pressure inside the pumping chamber and as a result the pumping chamber expands. In addition, some of the pressurized fluid in the pumping chamber is pushed to the compliance chamber through the inertia track and decoupler and the track's frictional resistance cause energy dissipation. Since the actuator that is used in our active mount replaces the decoupler to avoid modelling complexities the contribution of the decoupler in the hydraulic engine mount model is not considered.

2.1 Hydraulic Engine Mount Modelling

Figure 2-1 depicts a hydraulic engine mount without the decoupler. This mount can be modelled in terms of its elements' mathematical representations, i.e. compliances of the chamber, stiffness/damping rubber, and fluid inertia/resistance of the inertia track. The lumped model of the hydraulic mount is depicted in Figure 2-2. As it can be seen in lumped model, the stiffness and damping of the main rubber is represented by a physical spring and damper. The internal hydraulic parts of the engine mount are modelled as two cylinders with two accumulators, representing the pumping and compensation chamber compliances. The cylinders are connected to each other by a pipe that represents for the inertia track.

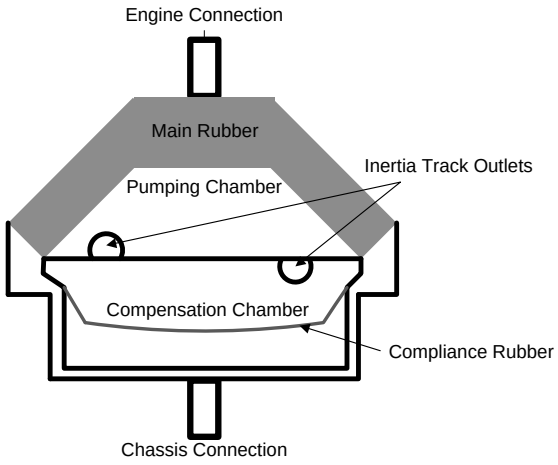

Figure 2-1: Hydraulic engine mount without decoupler.

Figure 2-1 is modelled by modifying Figure 1-8 into the lump model description in Figure 2-2.

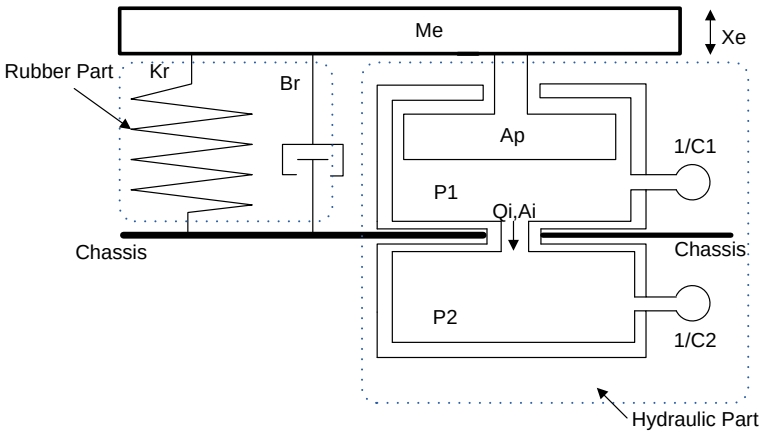

Figure 2-2: Lumped model of a hydraulic mount without decoupler.

In Figure 2-2, M_e is the effective mass of engine load on the mount, X_e is the engine displacement, A_r is the effective pumping area of the mount, Q_i is the flow rate of the fluid passing through the inertia track, C_1 and C_2 are the pumping chamber and compliance chambers compliances, K_r and B_r are the rubber stiffness and damping respectively.

Here, the upward motion of the engine is assumed positive. The engine mount fluid continuity relations is,

$$C_1\dot{P}_1 = -A_r\dot{X}_e - Q_i. \tag{2.1}$$

Equation (2.1) shows the relation between the motion of the piston in the upper cylinder, the fluid flow through the inertia track, and the pressure increase in the upper cylinder. The fluid flow through the inertia track escapes to the compliance chamber which can expand to hold the extra fluid. The fluid flow to the compliance chamber can be expressed in terms of its pressure increase and compliance as,(Equation (2.2)).

$$C_2\dot{P}_2 = Q_i. \tag{2.2}$$

The fluid inside the inertia track can be modelled by a finite mass M_i displaced as x_i. This mass moves in the inertia track because of the net hydraulic force of the upper and lower chambers (Figure 2-3). The motion of the fluid mass is expressed as

$$F_1 - F_2 = M_i\ddot{x}_i + b_i\dot{x}_i, \tag{2.3}$$

where $F_1$and F_2 are hydraulic forces and b_i is the viscous friction in the pipe. It should be noted that the flow in the inertia track is assumed laminar. The fluid flow introduced earlier is $Q_i = A_i\dot{x}_i$. dividing both sides of the Equation (2.3) by A_i and rearranging the result we have

$$\frac{F_1}{A_i} - \frac{F_2}{A_i} = \frac{M_i}{A_i}\frac{1}{A_i}(A_i\ddot{x}_i) + \frac{b_i}{A_i}\frac{1}{A_i}(A_i\dot{x}_i), \tag{2.4}$$

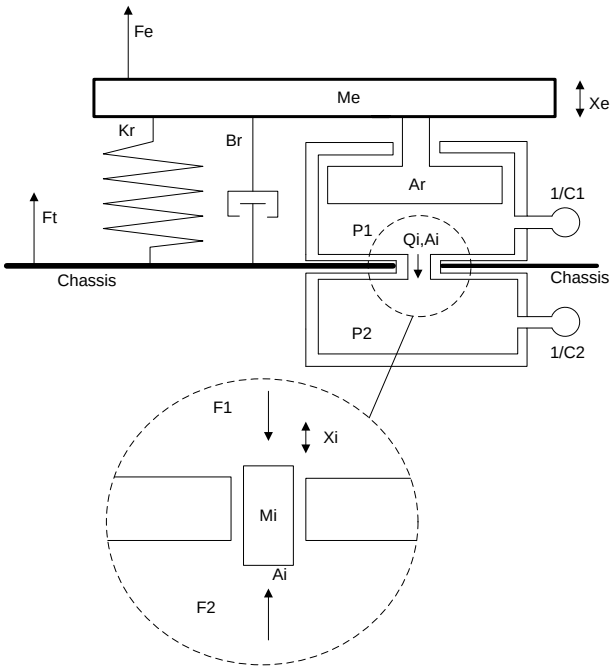

Figure 2-3: Modelling of fluid flow in the inertia track.

Notice that the left side in equation (2.4) is the pressure difference between the upper and lower chamber. So that we can rewrite (2.4) as (2.5)

$$P_1 - P_2 = \frac{M_i}{A_i^2}\dot{Q}_i + \frac{b_i}{A_i^2}Q_i. \tag{2.5}$$

Equation (2.5) describes the fluid flow in the inertia track due to the pressure difference. Here we get an analogy between $\dot{Q}_i$ and the acceleration of the mass, $\ddot{x}_i$, and an analogy between the flow rate Q_i and velocity of the mass, $\dot{x}_i$. Therefore we can define the inertia and the damping terms of the inertia track as $I_i = \frac{M_i}{A_i^2}$ and $R_i = \frac{b_i}{A_i^2}$. Equation (2.6) can be expressed as:

$$P_1 - P_2 = I_i\dot{Q}_i + R_iQ_i. \tag{2.6}$$

The two compliances in the upper and lower cylinders can be visualized as two small stiffnesses $k_1$and k_2.

$$\frac{1}{C_1} = \frac{k_1}{A_r^2}, \frac{1}{C_2} = \frac{k_2}{A_r^2}. \tag{2.7}$$

One way of solving the three coupled differential equations in (2.1), (2.2), and (2.6), is to use Laplace transformation. This makes the flow rate transfer function in terms of piston motion as:

$$Q_i(s) = \frac{-sA_rX_e(s)}{C_1[I_is^2 + R_is + \frac{1}{C_1} + \frac{1}{C_2}]}. \tag{2.8}$$

The pressure in the lower and upper chambers can also be expressed as,

$$P_2(s) = \frac{-A_rX_e(s)}{C_2C_1[I_is^2 + R_is + \frac{1}{C_1} + \frac{1}{C_2}]}, \tag{2.9}$$

$$P_1(s) = \frac{-A_r[I_iC_2s^2 + R_iC_2s + 1]X_e(s)}{C_2C_1\left[I_is^2 + R_is + \frac{1}{C_1} + \frac{1}{C_2}\right]}. \tag{2.10}$$

From Figure (2-3), the net force transmitted to the base is

$$F_T = K_rX_e + B_r\dot{X}_e - A_rP_1. \tag{2.11}$$

Substituting (2.10) in (2.11), the force transmitted becomes:

$$F_T(s) = [K_r + B_r s + \frac{A_r^2}{C_1} \frac{I_i s^2 + R_i s + \frac{1}{C_2}}{I_i s^2 + R_i s + \frac{1}{C_1} + \frac{1}{C_2}}] X_e(s). \tag{2.12}$$

So that the dynamic stiffness equation becomes

$$K_{dyn} = \frac{F_T(s)}{X_e(s)} = [K_r + B_r s + \frac{A_r^2}{C_1} \frac{I_i s^2 + R_i s + \frac{1}{C_2}}{I_i s^2 + R_i s + \frac{1}{C_1} + \frac{1}{C_2}}]. \tag{2.13}$$

In a typical hydraulic engine mount the main rubber damping is small and only affects the very high frequency responses (as we will see in the simulations later in this chapter). The dynamic stiffness equation is composed of adding three terms. The first two terms are the contribution of the rubber and the last one is the contribution of hydraulic components. If we neglect the effect of rubber damping in the frequency range of this study, and taking into account that $C_1 \ll C_2$, the dynamic stiffness equation predicts that at low frequency region the transmitted force and the engine displacement are related by $K_r + A_r^2/C_2$ and at high frequency (in our range of studies) the relation becomes $K_r + A_r^2/C_1$. Therefore, the mount is stiff in higher frequencies and soft in low frequencies. According to (2.13), the switching between soft and hard region occurs between $\omega_1 = \sqrt{\frac{1}{I_i C_2}}$ and $\omega_2 = \sqrt{\frac{1}{I_i C_1}}$. In other words, the hydraulic mount is a soft spring up to ω_1, passes an increasing trend in response for frequencies between ω_1, and ω_2 and finally, at ω_2, it is a hard mount.

The lump model of the hydraulic mount can be represented by a block diagram (Figure 2-4).

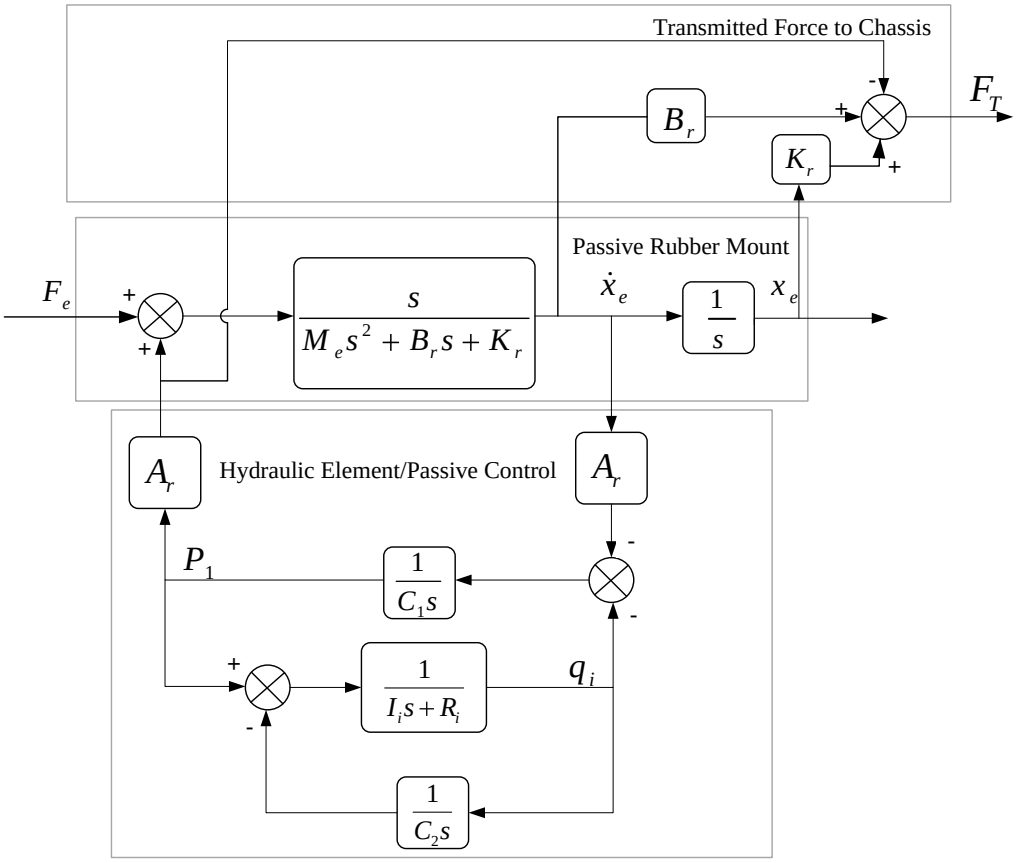

Figure 2-4: The block diagram of a passive hydraulic mount without a decoupler.

2.2 Dynamic Stiffness of Hydraulic Mount and the Transmissibility

As discussed earlier in Chapter 1, the transmitted force over the displacement of the mount is called dynamic stiffness. Equation (2.14) is dynamic stiffness formula of a mount.

$$K_d = \frac{F_T}{X_e}, \tag{2.14}$$

In this study the input displacement to the mount is oscillatory. Therefore, the force transmitted is also an oscillatory signal at the same frequency with a phase difference. The dynamic stiffness can be also written as

$$K_d(i\omega) = |K_d(i\omega)|e^{i\Phi_K(\omega)} = \\ |K_d(i\omega)|cos\big(\Phi_K(\omega)\big) + i|K_d(i\omega)|sin(\Phi_K(\omega)), \tag{2.15}$$

where $|K_d(i\omega)|$, and $\Phi_K(\omega)$ are the magnitude and the phase of dynamic stiffness $K_d(i\omega)$. The dynamic stiffness can also be written in terms of stiffness and damping as follows:

$$K_d(i\omega) = K_d(\omega) + \ iB_d(\omega)\omega, \tag{2.16}$$

where,

$$K_d(\omega) = |K_d(i\omega)|\ cos\big(\Phi_K(\omega)\big) = Real(K_d), \\ B_d(\omega) = \frac{|K_d(i\omega)|sin\big(\Phi_K(\omega)\big)}{\omega} = Img(K_d)/\omega. \tag{2.17}$$

where $K_d(\omega)$ is the true stiffness and $B_d(\omega)$ is the true damping of the mount. $K_d(i\omega)$, or dynamic stiffness, is the combination of both. Damping coefficient B is obtained by dividing the imaginary component over the frequency, and the real part is the stiffness component of the rubber and hydraulics, K (see Figure 2-5).

From Equation (2.13) it can be seen that the frequency response of the dynamic stiffness,$K_d(i\omega)$, will have an imaginary and real components. The resultant of the imaginary and real component gives the magnitude and phase of the dynamic stiffness.

$$Mag(K_d) = \sqrt{Img(K_d)^2 + Real(K_d)^2}\ , \\ \Phi_K = tan^{-1}\left(\frac{Img(K_d)}{Re(K_d)}\right). \tag{2.18}$$

Notice that the imaginary part reflects the combined contribution of fluid and rubber dampings.

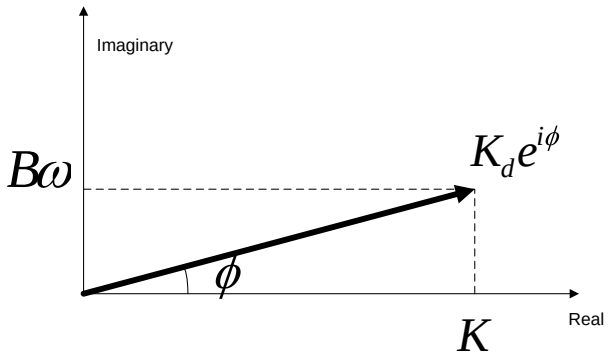

Figure 2-5: Real and imaginary components of the dynamic stiffness.

Transmissibility ratio, T_r, is another important characteristic of an engine mount; it shows the fraction of force transmitted from the engine to the chassis, or $T_r = (F_T/F_e)$. An ideal engine mount would have transmissibility equal to zero which means no force transfers from engine to chassis. The only possible way of making an ideal engine mount is through an active engine mount.

2.3 Hydraulic Engine Mount Experiment

In this section dynamic stiffness of a hydraulic engine mount (a mount without decoupler) is tested to show that the lumped model found in section 2.1 is in agreement with the test results. After that the parameters of the mount are extracted from the experimental data using a curve fitting method.

To test the dynamic stiffness of the hydraulic engine mount the lower part of the mount is attached to an electromagnetic shaker. The top of the mount is fixed to a rigid frame and a force sensor is placed between the rigid frame and the engine mount top. An LVDT (Linear Variable Displacement Transformer), measures the relative displacement between the top and bottom of the engine mount. The relative displacement represents the engine relative displacement with

respect to the chassis. Electromagnetic shaker enforces the relative displacement over the frequency range of interest and the force transmitted to the chassis is measured with the employed force sensor. Using the transmitted force and the displacement, the dynamic stiffness can be obtained. Here in this test the relative displacement of the mount is 0.1 mm peak to peak.

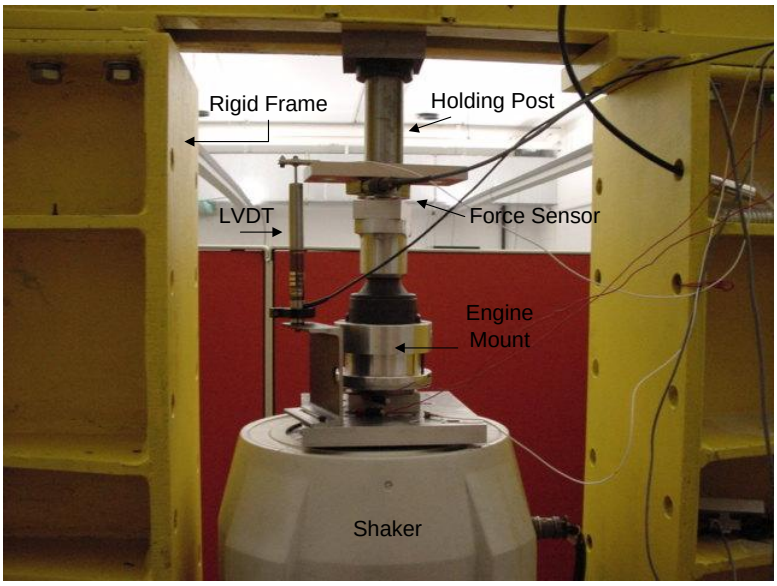

Figure 2-6: Dynamic stiffness test setup.

Figure 2-7 shows that the passive hydraulic mount has a switching frequency and a transition region and a flat shape in frequencies less than 5 Hz and in frequency 25-60 Hz (as discussed at the end of Section 2.1). Therefore the experimental data are used along the mathematical model to extract the parameters of the model. The simulation of the dynamic stiffness of the mount based on the model and the extracted parameters are shown in Figure 2-7. The model parameters are presented in Table 2-1. Results in Figure 2-7 demonstrates that the mathematical model is in close agreement with the physical system and therefore it is reliable. Having a reliable model we can proceed and study the behaviour of the hydraulic mount by simulation.

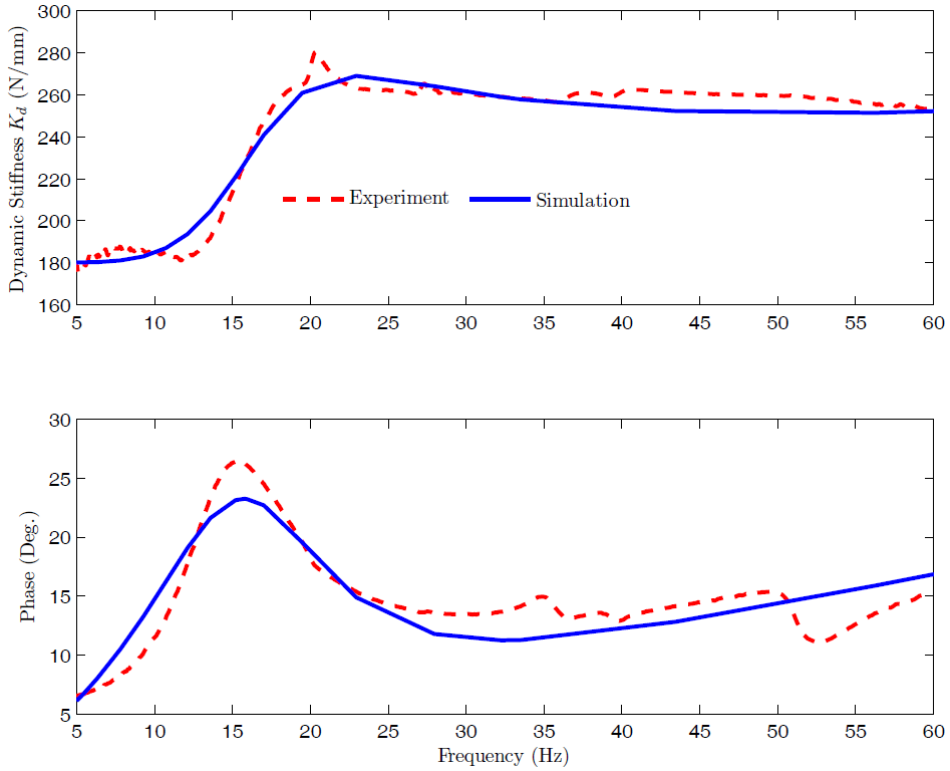

Figure 2-7: Dynamic stiffness of the mount. Experiment versus the model of hydraulic mount.

Table 2-1: The simulation parameters matching the experiments.

Parameter	Name	Value	Unit
Stiffness of pumping chamber	K_r	180	$\frac{N}{mm}$
Damping of pumping chamber	B_r	0.19	$\frac{N.s}{mm}$
Pumping area of pumping chamber	A_r	3650	mm^2
Compliance of pumping chamber	C_1	2.39×10^5	$\frac{mm^5}{N}$
Compliance of compensation chamber	C_2	2.03×10^7	$\frac{mm^5}{N}$
Inertia of track inertia	I_i	3.2×10^{-10}	$\frac{N.s^2}{mm^5}$
Resistance of track inertia	R_i	2.9×10^{-8}	$\frac{N.s}{mm^5}$

2.4 Hydraulic Engine Mount Simulation

In this section the model of the engine mount with the parameters that we obtained in the previous sections is simulated. The aim of these simulations is to validate the assumption made in obtaining the mathematical model. The simulation parameters are based on the realistic parameters of the mount.

The dynamic stiffness is often shown as a frequency response in a wide range of frequency. The hydraulic part of the engine mount is marked in the Figure 2-2. The effect of the hydraulic part on the dynamic stiffness is simulated and shown in Figure 2-8. The phase angle around the 90 degrees in the low frequency shows that the hydraulic mount dissipates energy and the amount of the dissipation increases as the excitation frequency reaches to the resonance

frequency of the mount. In high frequencies (the hard mount region), contribution of the hydraulics on the stiffness of the mount is about 64 (N/mm). Based on the phase angle it appears that the contribution of the hydraulic part at those frequencies is more stiffness and it does not damp significant amount of energy.

At 20 (Hz) resonance of the denominator of Equation (2.10) occurs. As a result the magnitude of the dynamic stiffness increases, and that result in high force transmission from the engine to the chassis. Figure 2-9 presents the same analysis in terms of real dynamic stiffness $Re(K_d)$, damping coefficient, B, and, imaginary dynamic stiffness, $Img(K_d)$.

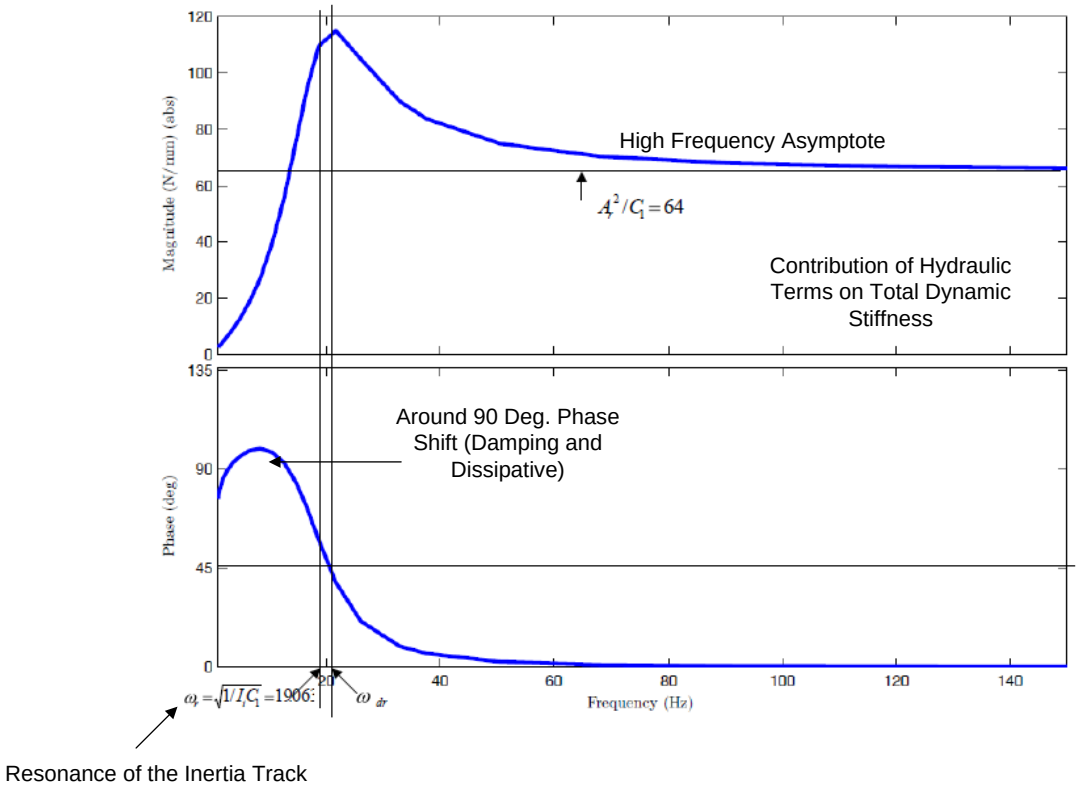

Figure 2-8: Hydraulic part of the dynamic stiffness.

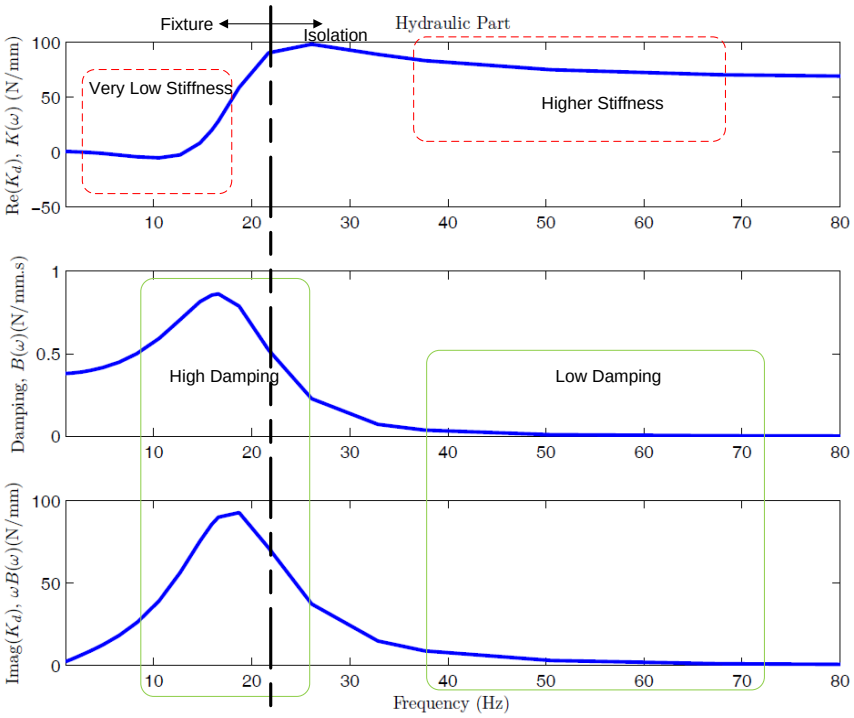

Figure 2-9: Contribution of the hydraulics in the real part of dynamic stiffness, damping coefficient, and imaginary part of the dynamic stiffness.

In Figure 2-10, the contribution of the stiffness of rubber, its damping, and hydraulic parts of the mount are compared together along that of the complete hydraulic dynamic stiffness.

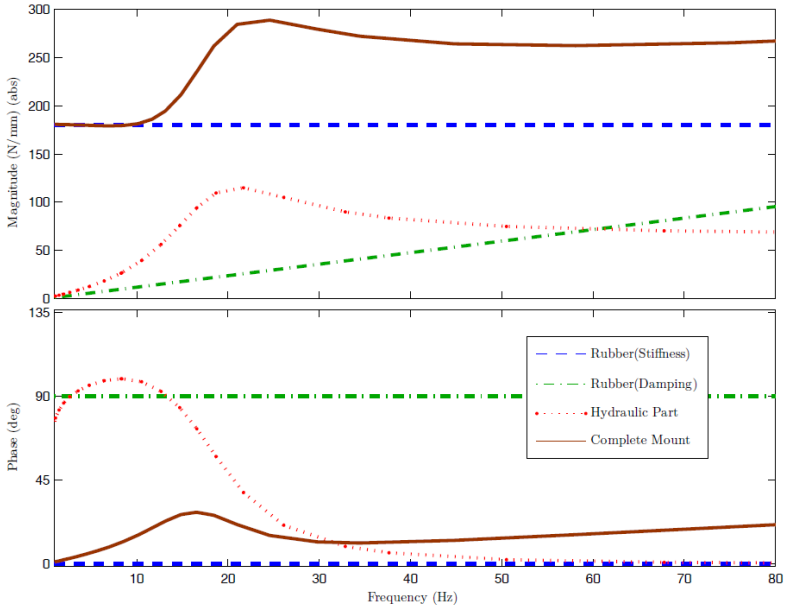

Figure 2-10: Comparison of the contribution of rubber damping, rubber stiffness, hydraulic part, and overall hydraulic mount.

Figure 2-11 presents the same information as depicted in Figure 2-8 in terms of real, imaginary and damping. This figure shows that at low frequencies (1-25 Hz) the fluid part plays an important role in generating damping which is required for the engine idle and road shocks. At high frequencies (25-80 Hz), even though the true stiffness of the mount remains constant but the contribution of the damping force of the rubber (related to the imaginary part of dynamic stiffness) is increasing by frequency. This result in high transmissibility and lowers the isolation performance.

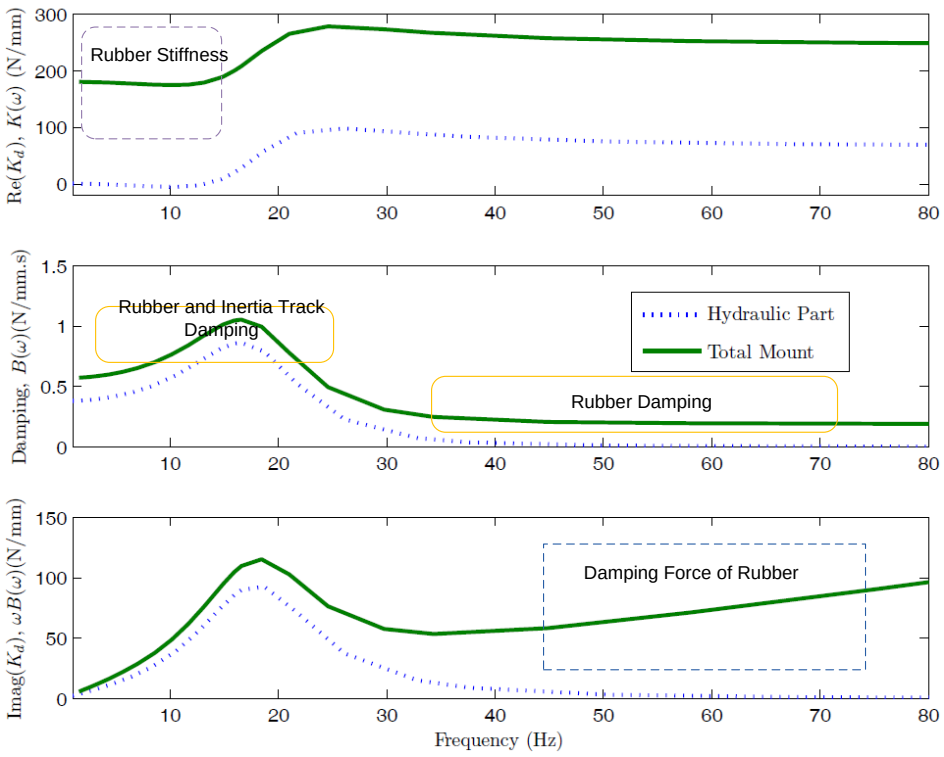

Figure 2-11: Contribution of the rubber part in the dynamic stiffness of engine mount and its comparison with the contribution of hydraulic part.

As seen before, the stiffness peak is around 20 Hz in the Figure 2-8 and that is due to resonance of the fluid mass in the inertia track. This can be seen in Figure 2-12 where the flow rate in the inertia track is simulated. It shows that at 20 Hz the fluid flow rate is max in the inertia track. The high flow rates relates directly to the damping due to the track resistance.

It is also interesting to see that the pressure in the upper and lower chamber increases at the resonance frequency but after the resonance the fluid flow rate in the track drops. Therefore the pressure in the lower chamber drops as there is low amount of fluid going into the lower chamber but the pressure in upper chamber stays high (see Figure 2-12, Figure 2-13, and Figure 2-14).

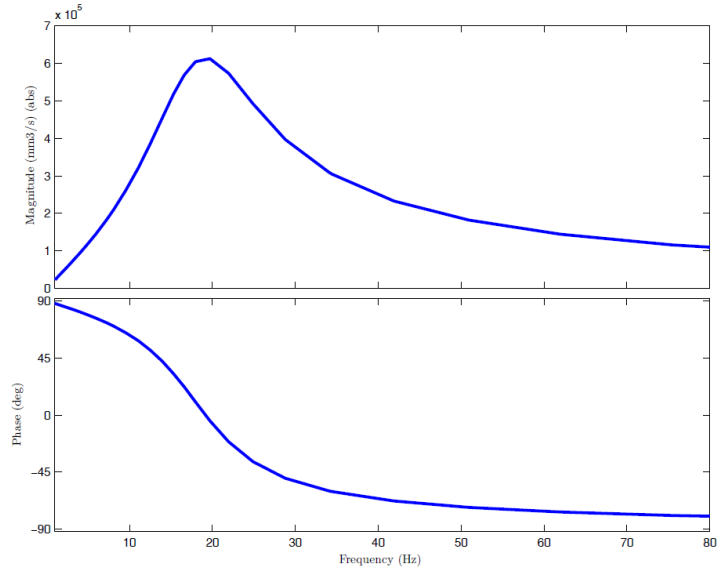

Figure 2-12: Flow rate in the inertia track.

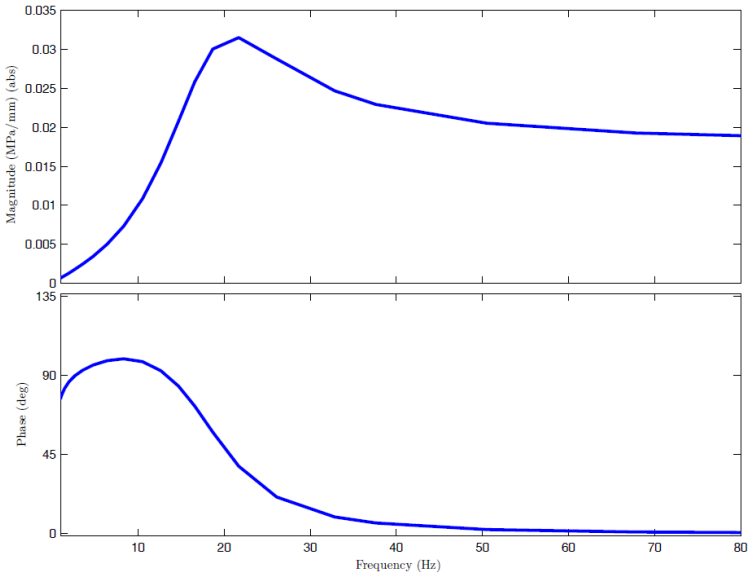

Figure 2-13: Pressure in the upper chamber.

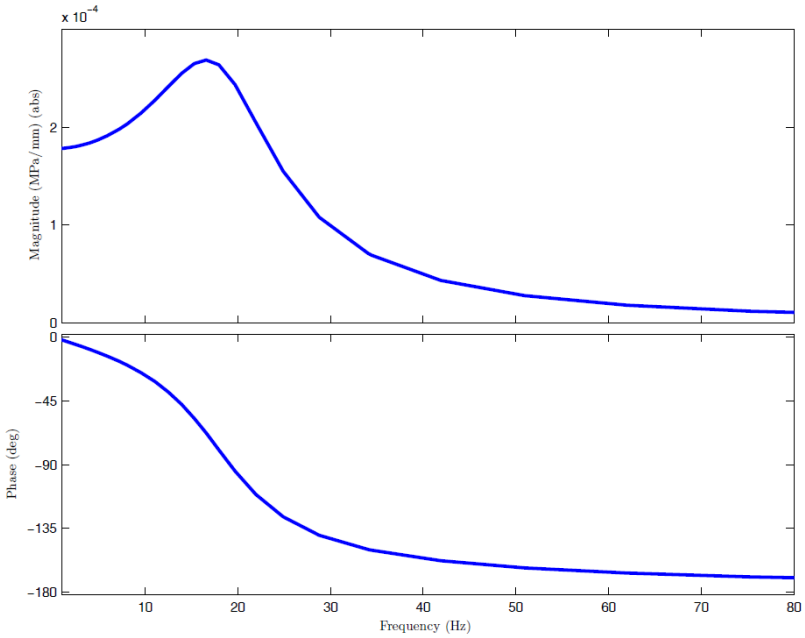

Figure 2-14: Pressure in lower chamber.

From the simulations in this chapter we come up with few conclusions about designing an engine mount. First that the transmitted damping force increases due to the rubber damping in high frequency (Remember from Chapter 1 that high force transmission deteriorates the isolation performance of a mount in high frequency). Also, the pressure in the upper chamber plays an important role in real part of the dynamic stiffness. Finally, the transmitted force around 20 Hz is high because the resonance of the inertia track occurs around this frequency.

A noise and vibration requirement along with the vehicle dynamics requirements are given in Figure 2-15. It is a list of the desired engine mount characteristics for each specific driving condition to address vehicle dynamics and ride comfort requirements. That information has been provided by General Motors for Cooper Standard Automotive for designing an engine mount.

The requirements are numbered from 1 to 7. By looking at the performance of the engine mount that we simulated in this chapter we can see that this mount meets the requirements 1, 5, 6 and somehow the requirement number 7. We can see that requirement 2, 3, 4 are not met by the hydraulic engine mount that is modelled in this chapter. Therefore to both address the vehicle dynamics requirements and noise and vibration requirements at the same time, design of a tuneable/controllable active engine mount is desired. The new engine mount must be capable of changing its characteristics based on the ride/load conditions, in response to sensors of the vehicle.

GM Future P/T Mount Requirements

Date: May 5, 2006 **By: Dennis Kinchen and Derek Hogland**

Applied to three P/T mount system architects: NTA (FWD), Transverse three-mount-to-cradle (FWD), longitudinal three-mount (RWD)

		Noise and Vibration Requirements				Vehicle Dynamics Requirements		
Customer Applications		Stationary vehicle in neutral or park with no accessory load at idle (no throttle input) 1	Stationary vehicle in drive with accessory load (A/C, headlights, rear defog) at idle (no throttle input) 2	Drive-away acceleration (moderate up to WOT) through the gears, rolling to highway speeds 3	Cruising at steady speeds (45 mph to highway speeds) in high gear 4	Cruising at steady speeds (45 mph to highway speeds) in high gear on a smooth road 5	Cruising at steady speeds (low to moderate speeds) in drive on a rough road 6	Cruising at steady speeds (low to moderate speeds) in drive on a smooth road with road impact 7
Vehicle and Subsystem Attributes	Engine Speed	650 to 800 erpm	600 to 750 erpm	1000 to 6000 erpm	1000 to 3000 erpm	1000 to 3000 erpm	1000 to 3000 erpm	1000 to 3000 erpm
	Vehicle Speed	zero	zero	5 to 85 mph	45 to 85 mph	45 to 85 mph	20 to 55 mph	20 to 55 mph
	Mount Preload	Static	Static plus nominal torque through driveline	Static plus up-to WOT torque through driveline in 1st or 2nd gear	Static plus nominal torque through driveline in high gear	Static plus nominal torque through driveline in drive (various gears)	Static plus nominal torque through driveline in drive (various gears)	Static plus nominal torque through driveline in drive (various gears)
	P-P	less than 0.1 mm	0.1 mm	0.1 mm	less than 0.1 mm	0.1 mm	greater than 1.0 mm	greater than 1.0 mm
	Frequency	5 to 20 Hz for idle lumpiness 20 to 40 Hz for idle shake	20 to 40 Hz	35 to 600 Hz	35 to 400 Hz	10 to 20 Hz	6 to 20 Hz	6 to 40 Hz
Powertrain Mount System Attributes	Mount Stiffness	Low stiffness in direction that reacts torque to enable low frequency rigid body mode (rotation around crankshaft)	Low stiffness in direction that reacts torque to enable low frequency rigid body mode (rotation around crankshaft)	Moderate rate build-up from nominal torque linear rate, high frequency dynamic stiffness not to exceed 3 times low frequency dynamic stiffness	Low stiffness with slight rate build-up from nominal torque linear rate, high frequency dynamic stiffness not to exceed 3 times low frequency dynamic stiffness	High stiffness dynamic rate in vertical direction to optimize apparent mass relative to suspension dynamics	High stiffness dynamic rate in vertical direction to optimize apparent mass relative to suspension dynamics	Moderate stiffness dynamic rate in vertical and fore/aft direction to optimize harshness relative to suspension dynamics
	Mount Damping	High damping in direction that reacts torque to enable decay of rigid body mode motion from random torque input	Low damping in direction that reacts torque to enable low frequency rigid body transmissibility (rotation around crankshaft)	Low damping in all directions to enable high frequency mount transmissibility	Low damping in all directions to enable high frequency mount transmissibility	High damping in vertical direction to optimize powertrain response to suspension dynamics	High damping in vertical direction to optimize powertrain response to suspension dynamics	Moderate damping in vertical and fore/aft direction to optimize harshness relative to suspension dynamics
Application of Technology		High Firing Torque or Random Idle Torque				Brand Image Performance Required		
		L4 diesel V6 diesel V8 diesel V6 cam-in-block gas engine V8 cam-in-block gas engine				Cadillac Buick GMC Hummer Saab		

Figure 2-15: GM's future mount requirements.

Chapter 3: DESIGN OF A SOLENOID-BASED ACTIVE ENGINE MOUNT

3.1 Presumption in this Specific Design

We saw in the previous chapter (in Section 2.4) that the pressure in the upper chamber plays an important role in the dynamic stiffness of the mount. Also few different works on active [**15**] [**14**] and semi-active [**12**] engine mounts has been introduced in Section 1.4 where the authors claimed that the performance of the mount is controlled by altering the pressure in the chambers. Therefore an actuation method is sought for altering the fluid pressure in the mount.

Previously, in active category, Piezo-electric actuators have been used. Piezo-electric actuators are light weight actuators with fast response time, and has been used in various vibration control problems. However they have low amplitude response and to be used in the engine mount problem, amplitude magnification methods must be designed that makes the manufacturing of the mount complex and expensive.

Voice coils have been used in the active engine mount problem. Voice coils (loud speakers) are built of a stationary permanent magnet and a moving winding. By changing the polarity of the winding, the permanent magnet creates a repulsive or attractive force and can make the winding go back-and-forth. Mathematical model of voice coils are well established and almost linear, therefore they are easy to control. The drawback to the voice coil is that they are expensive due to the permanent magnet of them.

In semi-active category, pressures of chambers are controlled by on-off solenoid valves and using pneumatic pressure and vacuum around the engine mount cylinders. This design

requires pneumatic pipelining and multiple solenoid valves and can potentially occupy a large space.

An alternative option that has been used in this thesis was turning a low-cost on-off solenoid into a controllable electromagnetic actuator. Solenoids are cheaper than voice coils but have a highly nonlinear equal. Moreover they are mostly used for on-off applications where there is no need for precise modelling. The solenoids are not designed for back-and-forth motion but rather for pull-in/hold and release.

3.2 The Principles of Solenoid Operation

A solenoid consists of a coil and a moving metal rod, also known as armature or plunger. The operation of solenoids is based on conversion of electrical energy into mechanical energy, and therefore solenoids are being considered as electromechanical actuators. Normally, the coil is a copper wire wound with a tiny pitch and placed in a metal (iron-based material) case, also known as a C-frame. The C-frame is a supporting structure that also contributes to the magnetic field produced by the coil.

Applying an electrical current to a solenoid coil generates a magnetic field or flux with intensity proportional to the current. The magnetic field pulls the plunger in. The reason for the plunger attraction is a ferromagnetic material with high magnetic permeability, whereas air which has very low magnetic permeability. Pulling the plunger inside closes the air gap and intensifies the field concentration inside the solenoid.

3.3 Design of the Actuator

A pull-in SolenoidCity's tabular low profile clapper solenoid Series S-16-264 with AWG number 21 (for details about this solenoid see Appendix A) was purchased and modified for use in this project. Figure 3-2 is the picture of the solenoid that is used in our work.

The plunger has a conical shape groove (improves the induced magnetic flux) and perfectly mates to a tapered metallic seats when it bottoms out. As the plunger moves inside to close the gap it compresses a spring which is improvised to return the plunger to its original position soon after the electrical current is disconnected.

The plunger of the solenoid is modified and turned into a flat plate (T-plunger). A return spring is selected and placed between the coil and plunger. Because the solenoid is meant to be in direct contact with the fluid in the upper chamber of the engine mount, a sealing rubber was fixed between the plunger and a holding metallic plate. Sealing rubber protects the coil from the water. The schematic of the solenoid is shown in Figure 3-1.

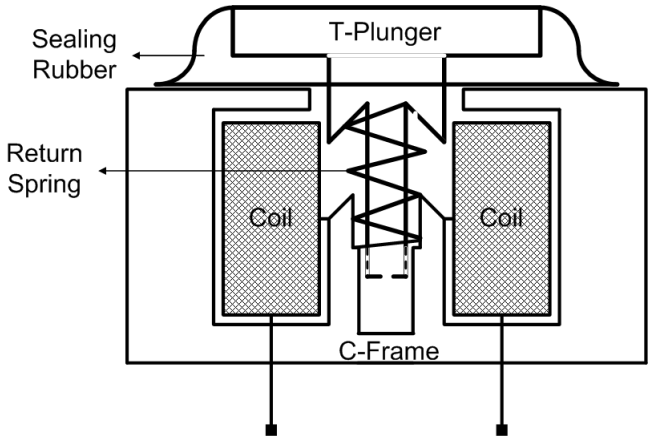

Figure 3-1: Schematic of an air-gap pull-type solenoid with sealing rubber and return spring.

A housing has been designed for this solenoid and it is placed between the compensation chamber and the pumping chamber Figure 3-3. The solenoid's moving part is in direct contact

with the pumping chamber fluid but it is isolated from the compensation chamber. The pressure inside the coil is the same as atmosphere as it is directly connected to the outside. The pressure on top of the plunger is the pressure of the pumping chamber. The fluid in compensation chamber is around the housing of the solenoid coil.

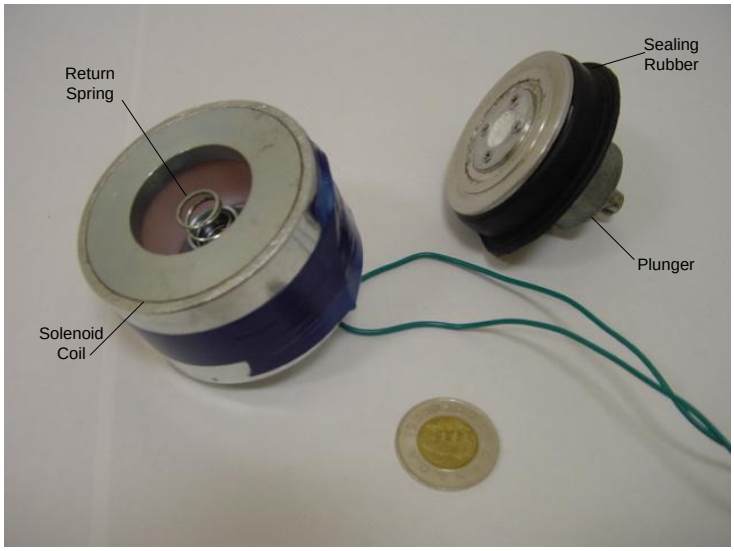

Figure 3-2: The modified solenoid that is used in the active engine mount.

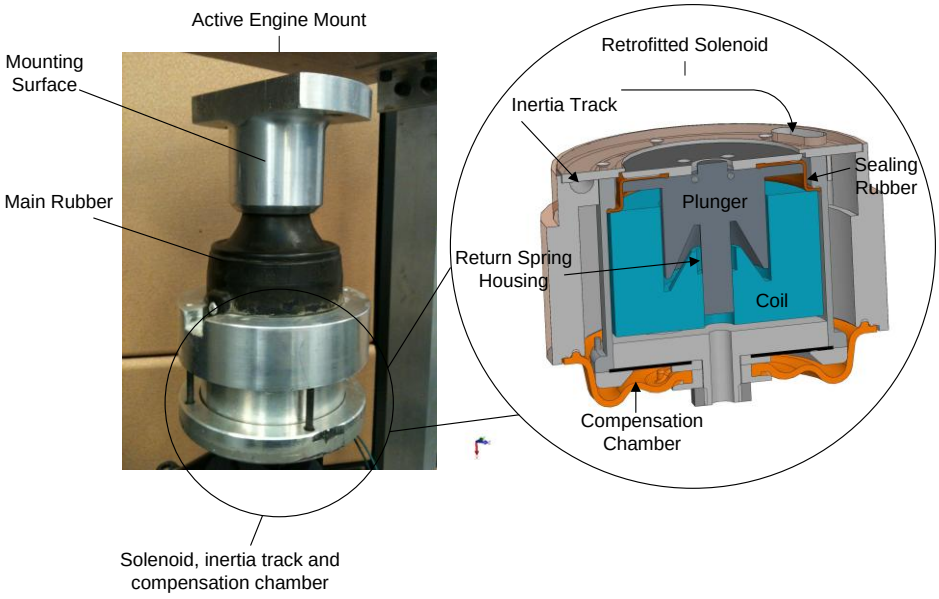

Figure 3-3: The solenoid-based active engine mount.

3.4 On-Off Solenoid to Actuator

The force of the solenoid, regardless of the polarity of the current in its coil, is downward towards the inside of the coil. As mentioned before, a return spring has been used to generate repulsive force to plunger. We used a technique to turn an on-off solenoid into a linear actuator. To accomplish this goal a bias current is fed into the coil of the solenoid. This generates a preloading on the spring.

Let us assume that this point, where the plunger is in static equilibrium in presence of spring's repulsive force and coil's attractive force, is the equilibrium or the operating point. Now if we increase the current the plunger goes towards to coil and if we decrease the current, the return spring pushes the plunger away from the coil. Therefore an oscillatory current plus a bias current can generate a back and forth motion in the plunger of the solenoid. Therefore the plunger can be used as a pump.

It must be mentioned that the amplitude of the oscillating current must be always less than the bias current; otherwise harsh nonlinearities will be created in the force of the solenoid. It must be also noticed that the addition of bias and oscillatory current must be always kept lower than what is required for completely closing the air-gap of the solenoid. Bottom out of the plunger with the coil is a nonlinear event and we want to avoid that.

3.5 Actuator Model Development

In our application, a solenoid actuator is utilized to pump and compress fluid in the pumping chamber. To most efficient way to simulate the interplay of the actuator and the hydraulic engine mount a mathematical model of the solenoid is needed to be later combined with the mount model. This model will also be an essential part of the controller design to drive the active mount

for desired performances at various frequencies. The steps for obtaining the actuator mathematical model are described in the followings:

Electromagnet Equation

A solenoid valve as explained earlier is composed of a coil and a plunger. The fundamentals of electromagnetic description of the solenoid valves is addressed in the literature [**26**] and [**22**]. This relation can be formulated as,

$$Ni_s(t) = H_c(t)l_c + H_g(t)l_g(t) + H_p(t)l_p, \tag{3.1}$$

where N is the number of the coil turns, $x_s(t)$ is the plunger motion, $H_c(t)$, $H_p(t)$, and $H_g(t)$, are the magnetic field intensity in the C-frame, in the plunger, and in the air gap. l_c, l_p, and l_g, are the mean lengths of the magnetic field in the C-frame, the plunger, and the air gap. $i_s(t)$ is the electrical current in the coil. The static magnetic force applied to the plunger, F_s, is

$$F_s = \frac{\partial W_m}{\partial x_s}, \tag{3.2}$$

where $W_m = \frac{1}{2}L(x_s, t)i_s^2(t)$ and $L(x_s, t)$ is the magnetizing inductance. The magnetizing inductance is

$$L(x_s\,, t) = \frac{N\Phi(x_s, t)}{i_s(t)}. \tag{3.3}$$

The magnetic flux can be calculated from,

$$\Phi = \frac{N i_s(t)}{\Re_p + 2\Re_g + \Re_c}, \tag{3.4}$$

where $\Re_p$, $\Re_g, \Re_c$ are the reluctances of the ferromagnetic materials of plunger, air-gap, and stationary core. The mathematical description of the reluctances are

$$\Re_p = \frac{l_p}{\mu_0 \mu_p A_e}, \tag{3.5}$$

$$\Re_g = \frac{\frac{l_g}{2}}{\mu_0 A_e},$$

$$\Re_c = \frac{l_a}{\mu_0 \mu_c A_e},$$

where μ_0 is the permeability coefficient of the air, and μ_c and μ_p are the permeability coefficient of the core and the armature. A_e is the effective cross section area through which the magnetic flux is flowing. $\frac{l_g}{2}$ can also be expressed as $\frac{l_g}{2} = x_0 + x_s(t)$, where constant x_0 is the half of the air gap when the current $i_s(t) = cte$, and the coil is magnetized with a constant current. From (3.3) and (3.4), the magnetizing inductance $L(x_s, t)$ can be expressed as

$$L(x_s, t) = \frac{N^2 \mu_0 \mu_p \mu_c A_e}{l_p \mu_c + 2\mu_p \mu_c [x_0 + x_s(t)] + l_c \mu_p}. \tag{3.6}$$

Therefore, combining (3.6) and (3.2), the magneto static force becomes

$$F_s(x_s, t) = \frac{N^2 \mu_0 \mu_p^2 \mu_c^2 A_e i_s^2(t)}{(l_p \mu_c + 2\mu_p \mu_c [x_0 + x_s(t)] + l_c \mu_p)^2} \tag{3.7}$$

To simplify (3.7), new terms, α, β, and γ, are which are defined in (3.8) as,

$$\alpha = N^2 \mu_0 \, \mu_p^2 \, \mu_c^2 \, A_e,$$
$$\beta = l_p \mu_c + \, 2\mu_p \mu_c x_0 + \, l_c \mu_p, \tag{3.8}$$
$$\gamma = 2\mu_p \mu_c.$$

so that the force applied by the magnetic field on the solenoid armature is,

$$F_s(x_s, i_s) = \frac{\alpha i_s^2(t)}{\left(\beta + \gamma x_s(t)\right)^2}. \tag{3.9}$$

In order to use the force equation, the values for α, β, and γ, are needed. Solenoid manufacturing companies cannot provide these values since analytical models are not the basis of their products design and it is not demanded by their customers. Instead, they publish data-sheets which are the curves of the measured force on a plunger based on its position at a few applied currents to the coil. These data-sheets are sufficient for industrial applications where the main applications of solenoids are on/off switches. Although, the curves in the solenoid datasheets enable us to estimate $\alpha, \beta,$ and γ. However, the procedure does not have sufficient accuracy. To identify more reliable values, experiments must be conducted.

Actuator Dynamics

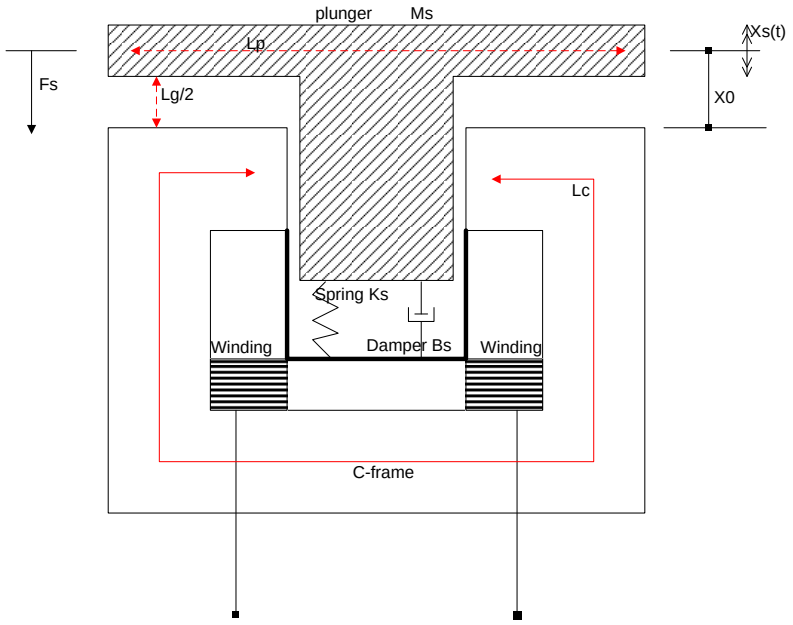

Figure 3-4: Lump model of an air-gap type solenoid.

A lumped model of the actuator mechanical components is depicted in Figure 3-4. In this model the plunger mass and the sealing rubber and return spring that are contributing to the stiffness and damping of the reciprocating system are represented by m_s, k_s and b_s. The equation of motion of the solenoid plunger can be written as,

$$F_s(t) - b_s\dot{x}_s(t) - k_s x_s(t) = m_s\ddot{x}_s(t). \tag{3.10}$$

As mentioned before, the solenoid coil can only generate attraction force which is only toward the center of the coil (downward here). It is because for attraction of ferromagnetic materials the polarity of the magnetic field is not important. In order to generate a reciprocating motion in the plunger, we need a return force provided by the pre-compressed return spring. The pre-compression of the spring is created by a bias current through the coil. The bias current should be high enough to compress the spring to an extent that strong oscillation of the plunger around that

point is feasible, and at the same time it should not be so large as to make the plunger bottom out. In conclusion, there is always a one-directional current going through the coil and its amplitude is modulated adding another oscillating current to that.

The forcing function which is applied on the plunger by the magnetic field is given in (3.9) . Combining the two equation results:

$$-\frac{\alpha i^2(t)}{\left(\beta+\gamma x_s(t)\right)^2} = m_s\ddot{x}_s(t) + b_s\dot{x}_s(t) + k_s x_s(t). \tag{3.11}$$

Equation (3.11) has nonlinear terms on the left hand side. The nonlinearity is on the square current and on the inverse of the square of displacement. These nonlinearities make combining it with the hydraulic mount equations difficult. It helps if we can linearize it to depend only on electrical current.

Model Linearization

.In this application, linearization is a reasonable model simplification by taking into consideration that at high frequencies (10-100 Hz), which is the vibration isolation frequency that the decoupler (our actuator is replaced for the decoupler) is dominant, the range of motion of the plunger is very small (less than 0.5 mm). Therefore the inverse square of displacement does not affect the denominator of the nonlinear forcing function of the Equation (3.11). Moreover, the permeability factor, $\mu\ (H/m)$, of ferrous material lies in the range 10^{-2}-10^{-5} which indicates (referring to (3.8)), that $\gamma \ll \beta$. Then the force function can be simplified to

$$F_s(t) = -\frac{\alpha i_s^2(t)}{\beta^2}. \tag{3.12}$$

Operating regions of the solenoids can be divided into a low current linear region and a high current saturated operating region. In the saturation region the magnetic field in the ferromagnetic material saturates. By keeping the current levels low, we can avoid entering the saturated region. Because the range of applied current is low in this application, $i_s < 1A$, and the fact that the Equation (3.12) is a parabola we can write the Equation (3.12) as:

$$F_s(i) = -\frac{\alpha i^2(t)}{\beta^2} = -\frac{2\alpha i_s}{\beta^2} i + \frac{\alpha i_s^2}{\beta^2}. \tag{3.13}$$

The linear force function can then be expressed as

$$F_s(i(t)) = -\frac{2\alpha i_s}{\beta^2} i(t) + f = -G_s i(t) + f. \tag{3.14}$$

where G_s and b are constant gains and are dependent on the bias current i_s.

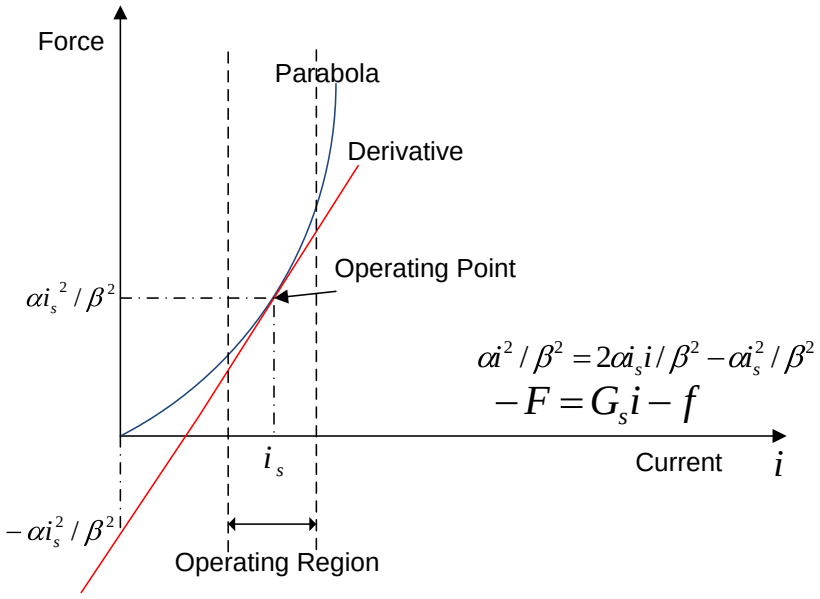

Figure 3-5: Linearization of the solenoid force function.

Model Identification

Using (3.14) and (3.11), the equation of motion of solenoid plunger can be written as:

$$-G_s i(t) + f = m_s \ddot{x}_s(t) + b_s \dot{x}_s(t) + k_s(x_s(t) + x_c), \tag{3.15}$$

where

$$f = k_s x_c, \tag{3.16}$$

and x_c is a pre-compression to adjust the constant force f. Therefore equation (3.15) is simplified into

$$-G_s i(t) = m_s \ddot{x}_s(t) + b_s \dot{x}_s(t) + k_s x_s(t), \tag{3.17}$$

Therefore the dynamic force of the solenoid can be modeled by a gain G_s and i is the amplitude of the oscillatory current.

The mass, m_s, is measured using a scale and the spring stiffness, k_s, is found by performing a static force/deflection test using dead weights. Based on our measurements, the plunger mass is $m_s = 0.2$ (Kg), and the spring/rubber stiffness is $k_s = 5.9$ (N/mm). The block diagram of the experimental setup is depicted in Figure 3-6 and the components used in this experiment are listed in Table 3-1.

Our approach is to excite the solenoid plunger with different oscillating currents and measure the acceleration of the tip of the plunger. The Simulink and Real-Time Workshop (RWT) are run on one PC which is interfaced by a Data Acquisition card (Sensoray 626). The shaker acceleration is sensed and sent to the Simulink. The shaker is programmed to oscillate

with a constant peak acceleration value of $1(gn)$, or $9.81\ \left(\frac{m}{s^2}\right)$. The acceleration of the shaker is translated into current command and is sent to the solenoid coil, and by sweeping the oscillations we can excite the solenoid plunger with the same frequency as the shaker.

To formulate the relations, equation (3.15) can be transformed to Laplace domain,

$$\frac{X_s}{I_s} = \frac{-G_s}{m_s s^2 + b_s s + k_s}. \tag{3.18}$$

Also, to be able to use the experimental results from the accelerometer equation (3.15) is converted to:

$$\frac{s^2 X_s}{I_s} = \frac{-s^2 G_s}{m_s s^2 + b_s s + k_s}. \tag{3.19}$$

Table 3-1: Instruments used in frequency response analysis of the solenoid.

Device	Model
Solenoid	Magnetic Sensor Systems, Pull-type Low Profile Clapper Solenoid, AWG#21
PWM Servo Amplifier	Advanced Motion Controls, 16A20AC
Plunger Accelerometer	Dytran 3035 AG
Shaker Accelerometer	Dytran 3035 AG
Shaker	VTS, VG 100-8
Shaker Controller System	LDS DACTRON LASER
Shaker Power Supply	Techron 5507
Sensor Charge Amplifier	Dytran 4105C, Current Source

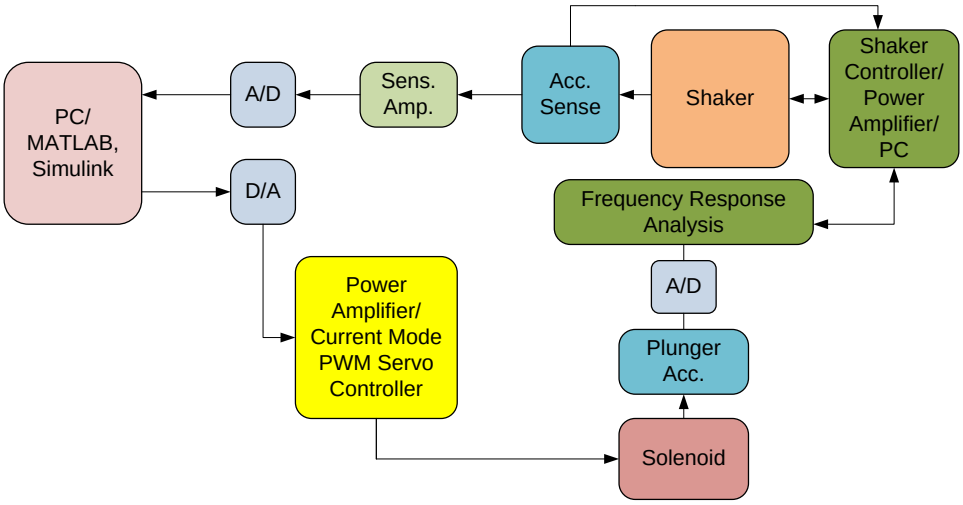

Figure 3-6: Schematic of frequency response test of the solenoid plunger.

We performed twenty frequency response tests with different bias and amplitude current, and with range of frequency sweeps between 10 and 45 (Hz). We measured the acceleration of the plunger in response to sinusoidal current input into the solenoid coil. The tests are performed to find the damping, b_s, and the gain of the actuator, G_s. The natural frequency of the solenoid is found to be close to $172\ \left(\frac{rad}{sec}\right)$ or 27.37 (Hz).

$$\omega_n = \sqrt{\frac{k_s}{m_s}} \approx 172\ \left(\frac{rad}{sec}\right). \tag{3.20}$$

The graphs show that the results can be fitted into a transfer function similar to (3.19). By selecting the gain $G_s = 6.4\ (N/A)$ and damping $b_s = 30\ \left(N.\frac{m}{s}\right)$, we find that the results closely match the test results. We can assume therefore that the plunger/solenoid equation of motion in Laplace domain is

$$[0.2s^2 + 30s + 5900]s^2X_s(s) = -6.4s^2I(s). \tag{3.21}$$

Now that the linear model of the solenoid is identified, in the next chapter, we couple the model of passive and active elements to find the linearized governing equations of the mount dynamics.

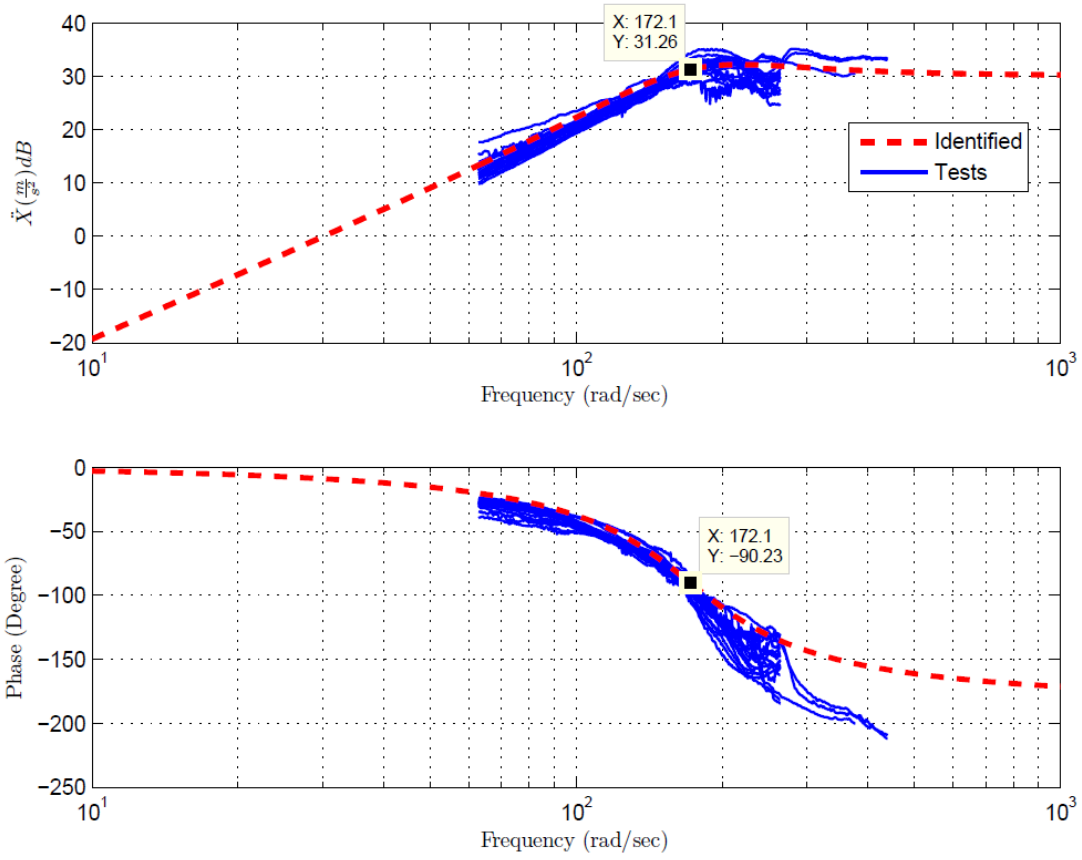

Figure 3-7: Frequency response of the acceleration of the plunger to the current (solid lines) vs. the Bode diagram of the identified linearized second order model (dashed line).

Chapter 4: MODELLING OF SOLENOID-BASED ACTIVE HYDRAULIC ENGINE MOUNT

As discussed in Chapter 1, modelling of hydraulic engine mounts has been studied by different authors. In Chapter 2, we modelled the hydraulic engine mount without decoupler. The important terms in the dynamic stiffness has been studied as well. In Chapter 3, we came into the design of a solenoid-based hydraulic mount. Therefore we identified the linear model of the solenoid in that Chapter. In this chapter, we integrate the previously developed governing equations of the hydraulic mount with the solenoid. After that we will analyse the effect of the plunger motion on the dynamics stiffness and transmissibility of the mount.

4.1 Active Engine Mount Modelling

The active mount of this study is designed to isolate chassis from engine excitation. To derive the mathematical model of this engine mount, we assume that the chassis is stationary. The main goal is to find a closed-form linear transfer function for engine force transmissibility and dynamic stiffness.

Figure 4-1 shows the lumped model of our active engine mount. Taking the positive direction upward in our reference coordinate frame, the motion of the solenoid plunger can be expressed as,

$$-G_s i - A_s P_1 = k_s x_s + b_s \dot{x}_s + m_s \ddot{x}_s. \tag{4.1}$$

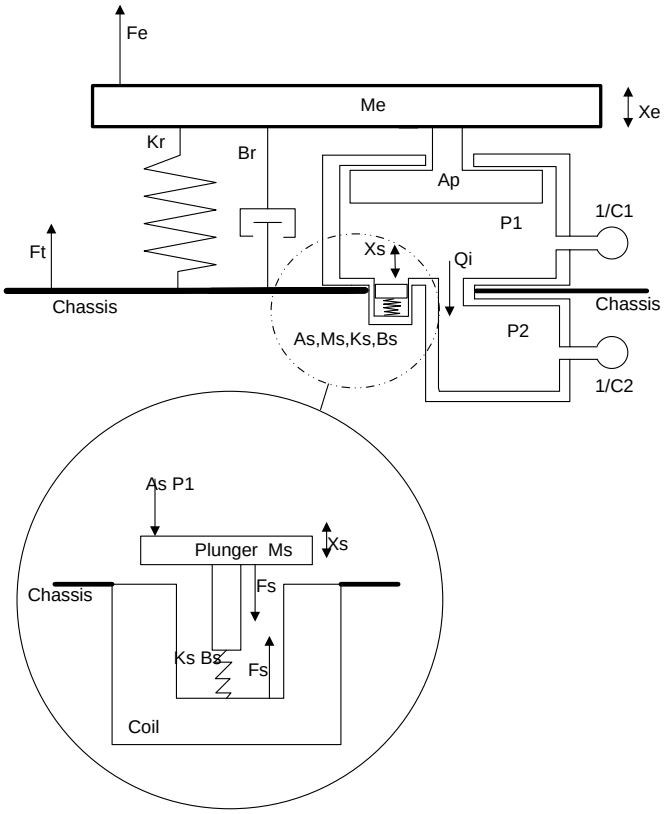

Figure 4-1: Lumped model of the active engine mount with a zoom on the plunger and coil's effective connection to the chassis.

Similar to our approach in chapter two, the engine is modelled as a mass. The equation of motion of the engine displacement is,

$$F_e - K_r x_e - B_r \dot{x}_e + A_r P_1 - \hat{F}_s = M_e \ddot{x}_e. \tag{4.2}$$

The transmitted force to the chassis is,

$$F_T = K_r x_e + B_r \dot{x}_e - A_r P_1 + k_s x_s + b_s \dot{x}_s - \hat{F}_s, \tag{4.3}$$

where $\hat{F}_s$ is the representation of the solenoid force and is equal to $-G_s i$, (G_s is a constant value), F_e and F_T are engine dynamic forces and transmitted force to the chassis, respectively, M_e is the

mass of engine or a fraction of the engine mass (depending on the number of the mounts and bushing that support it), x_e is the engine displacements, K_r and k_s are bulk rubber stiffness and solenoid stiffness, respectively, B_r is the bulk rubber damping, and b_r is the solenoid damping identified in the previous chapter, P_1 is dynamic pressure inside the pumping chamber, and A_r is the effective area of pumping chamber.

The equations of the hydraulic part of the engine mount are presented in Chapter 2 (Equations (2.1), (2.2), and (2.6)). From combining (2.1), (2.2) and (2.6), we obtain the relationship between P_1 and P_2 as

$$P_1 = P_2 + R_i C_2 \dot{P}_2 + I_i C_2 \ddot{P}_2. \tag{4.4}$$

Taking the Laplace transform from (4.4), the pressure transfer function is,

$$\frac{P_2}{P_1} = \frac{1}{I_i C_2 s^2 + R_i C_2 s + 1} \tag{4.5}$$

Taking into account the volume expansions and contractions of the pumping and compensation chamber, as well as solenoid plunger motion, and by assuming that the fluid is not compressible, we can adapt the Equation (2.1) into,

$$C_1 \dot{P}_1 + C_2 \dot{P}_2 = -A_r \dot{x}_e + A_s \dot{x}_s, \tag{4.6}$$

where x_s is the solenoid displacement, and A_s is the plunger pumping area. The equation of motion of the solenoid plunger is,

$$-G_s i - A_s P_1 = k_s x_s + b_s \dot{x}_s + m_s \ddot{x}_s, \tag{4.7}$$

where m_s is the plunger mass. Therefore, the pressure in the pumping chamber can be written as

$$P_1 = \frac{[A_s X_s - A_r X_e][I_i C_2 s^2 + R_i C_2 s + 1]}{C_2 + C_1[I_i C_2 s^2 + R_i C_2 s + 1]}, \tag{4.8}$$

where, for simplicity of the equations, we introduce $\Psi = \frac{I_i C_2 s^2 + R_i C_2 s + 1}{C_2 + C_1[I_i C_2 s^2 + R_i C_2 s + 1]}$. Therefore, the pressure equation can be expressed as follows:

$$P_1 = A_s X_s \Psi - A_r X_e \Psi. \tag{4.9}$$

Combining (4.2) and (4.9), the equation of motion of engine mass due to the engine force F_e, and the force generated by the solenoid actuation is:

$$F_e = [M_e s^2 + B_r s + K_r + A_r^2 \Psi] X_e + G_s I_s - A_r A_s \Psi X_s \tag{4.10}$$

The armature position equation in Laplace domain is

$$-P_1 A_s - G_s I_s(s) = [m_s s^2 + b_s s + k_s] X_s(s) \tag{4.11}$$

Substituting P_1 from equation (4.9) into equation (4.11), results,

$$-G_s I_s = -[m_s s^2 + b_s s + (k_s + A_s^2 \Psi)] X_s + A_s A_s \Psi X_e, \tag{4.12}$$

or

$$\frac{(G_s I_s - A_s A_r \Psi X_e)}{X_s} = -[m_s s^2 + b_s s + (k_s + A_s^2 \Psi)]. \tag{4.13}$$

Now X_s can be expressed in terms of current and X_e:

$$X_s = \frac{A_s A_r \Psi X_e - G_s I_s}{m_s s^2 + b_s s + (k_s + A_s^2 \Psi)}. \tag{4.14}$$

Knowing the relation of P_1 with X_e and I_s as follows, Equation (4.3) becomes,

$$P_1 = \left[-A_r\Psi + \frac{(A_s^2 A_r \Psi)}{m_s s^2 + b_s s + (k_s + A_s^2\Psi)}\right] X_e - \left[\frac{G_s A_s \Psi}{m_s s^2 + b_s s + (k_s + A_s^2\Psi)}\right] I_s, \tag{4.15}$$

Then, the transmitted force to the chassis is,

$$F_T = \left[K_r + B_r s + A_r^2\Psi + \frac{(k_s + b_s s)(A_s A_r \Psi) - A_s^2 A_r^2 \Psi^2}{m_s s^2 + b_s s + (k_s + A_s^2\Psi)}\right] X_e + \left[G_s + G_s \frac{A_r A_s \Psi - (k_s + b_s s)}{m_s s^2 + b_s s + (k_s + A_s^2\Psi)}\right] I_s. \tag{4.16}$$

The interaction between the engine unbalance forces and the active elements of the engine mount can be expressed by the following equation,

$$F_e = \left[M_e s^2 + B_r s + K_r + A_r^2 - \frac{A_s^2 A_r^2 \Psi^2}{m_s s^2 + b_s s + (k_s + A_s^2\Psi)}\right] X_e + G_s \left[1 + \frac{A_r A_s \Psi}{m_s s^2 + b_s s + (k_s + A_s^2\Psi)}\right] I_s. \tag{4.17}$$

The dynamic stiffness function for our active engine mount is,

$$\frac{F_T}{X_e} = \left[K_r + B_r s + A_r^2\Psi + \frac{(k_s + b_s s)(A_s A_r \Psi) - A_s^2 A_r^2 \Psi^2}{m_s s^2 + b_s s + (k_s + A_s^2\Psi)}\right] + G_s \left[1 + \frac{A_r A_s \Psi - (k_s + b_s s)}{m_s s^2 + b_s s + (k_s + A_s^2\Psi)}\right] \frac{I_s}{X_e}. \tag{4.18}$$

Figure 4-2 is the block diagram of the solenoid-based active hydraulic engine mount. Next, we derive the equations of the active mount in state-space. By having the equations of motion in state-space domain, we can easily observe the state variables of the system.

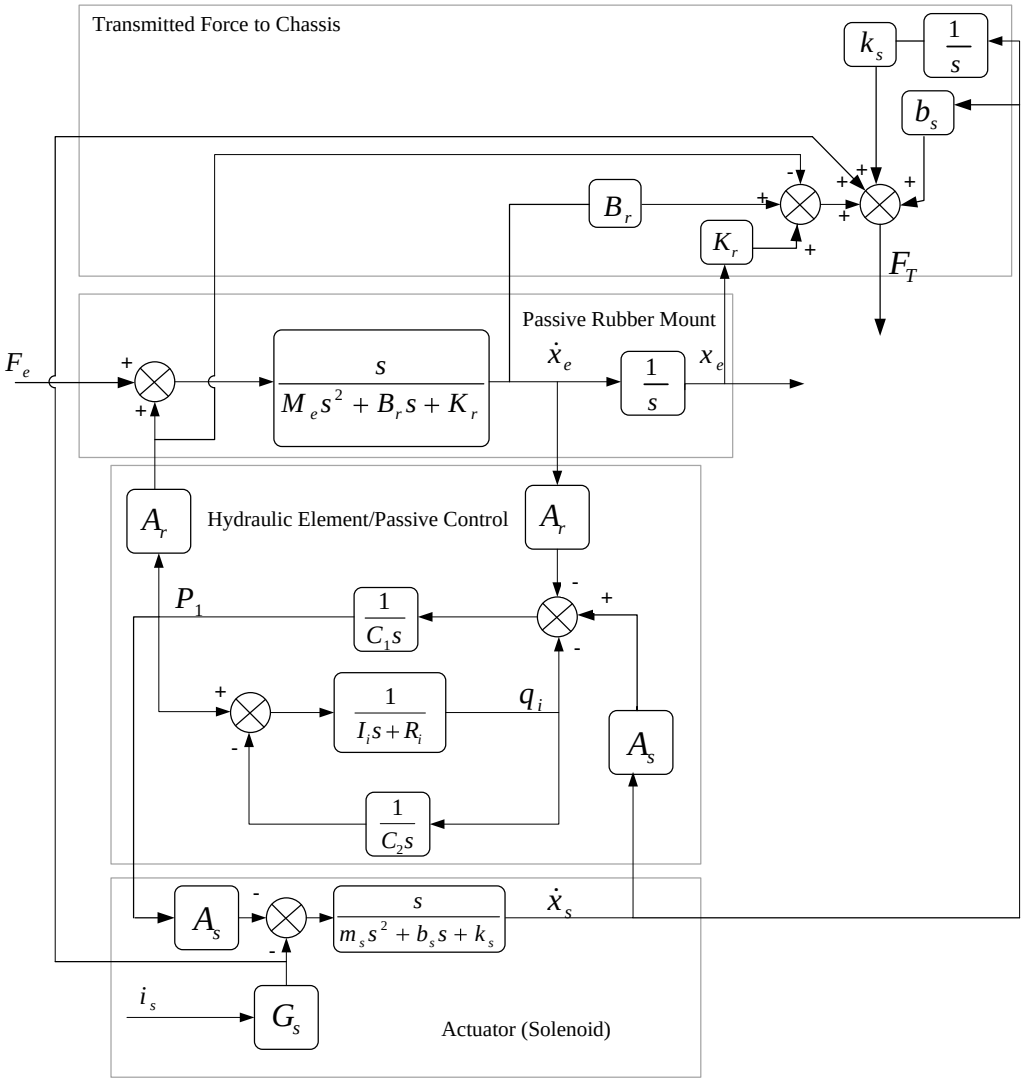

Figure 4-2: Block diagram of the analytical model of the active engine mount.

4.2 Active Engine Mount Modelling in State-Space

Hydraulic Engine Mount Modelling in State-Space Domain

The governing equations of a hydraulic mount where found in Chapter 2. Expressing the equation of motion in state-space format provides an easier way to investigate the interplay of the engine mount components. The complete governing equation of the hydraulic engine mount in state-space form is presented in (4.19) and (4.20).

$$\begin{bmatrix}\dot{x}_e\\ \ddot{x}_e\\ \dot{p}_1\\ \dot{p}_2\\ \dot{q}_i\end{bmatrix}=\begin{bmatrix}0 & 1 & 0 & 0 & 0\\ -\frac{K_r}{M_e} & -\frac{B_r}{M_e} & \frac{A_r}{M_e} & 0 & 0\\ 0 & -\frac{A_r}{C_1} & 0 & 0 & -\frac{1}{C_1}\\ 0 & 0 & 0 & 0 & \frac{1}{C_2}\\ 0 & 0 & \frac{1}{I_i} & -\frac{1}{I_i} & -\frac{R_i}{I_i}\end{bmatrix}\begin{bmatrix}x_e\\ \dot{x}_e\\ p_1\\ p_2\\ q_i\end{bmatrix}+\begin{bmatrix}0\\ \frac{1}{M_e}\\ 0\\ 0\\ 0\end{bmatrix}[F_e], \tag{4.19}$$

$$\begin{bmatrix}F_T\\ x_e\\ \dot{x}_e\\ p_1\\ p_2\\ q_i\end{bmatrix}=\begin{bmatrix}K_r & B_r & -A_r & 0 & 0\\ 1 & 0 & 0 & 0 & 0\\ 0 & 1 & 0 & 0 & 0\\ 0 & 0 & 1 & 0 & 0\\ 0 & 0 & 0 & 1 & 0\\ 0 & 0 & 0 & 0 & 1\end{bmatrix}\begin{bmatrix}x_e\\ \dot{x}_e\\ p_1\\ p_2\\ q_i\end{bmatrix}. \tag{4.20}$$

The states of the system are presented in lower-case letters to remind that they are in time domain (e.g. q_i instead of Q_i).

Active Engine Mount Modelling in State-Space Domain

An active engine mount is a multi-input single-output (MISO) system. The engine unbalance force and the current to the solenoid are the inputs, and the transmitted force is the output. We also add the states of the system to the output list (e.g., chamber pressures, inertia track flow, displacements.). This can be a means of sizing and sensor selecting for the purpose of mount optimization and control. Therefore, we are dealing with a multi-input multi-output (MIMO) system.

Using the state-space form given previously in (4.19) and (4.20) and the newly introduced active mount relations we can find the state-space representation of the active hydraulic mount in this section. Therefore by coupling equations (4.6), and (4.7), we derive equations (4.21) and (4.22) as the governing equation of the whole system.

$$\begin{bmatrix}\dot{x}_e\\ \ddot{x}_e\\ \dot{p}_1\\ \dot{p}_2\\ \dot{x}_s\\ \ddot{x}_s\\ \dot{q}_i\end{bmatrix}=\begin{bmatrix}0 & 1 & 0 & 0 & 0 & 0 & 0\\ -\frac{K_r}{M_e} & -\frac{B_r}{M_e} & \frac{A_r}{M_e} & 0 & 0 & 0 & 0\\ 0 & -\frac{A_r}{C_1} & 0 & 0 & 0 & \frac{A_s}{C_1} & -\frac{1}{C_1}\\ 0 & 0 & 0 & 0 & 0 & 0 & \frac{1}{C_2}\\ 0 & 0 & 0 & 0 & 0 & 1 & 0\\ 0 & 0 & -\frac{A_s}{m_s} & 0 & -\frac{k_s}{m_s} & -\frac{b_s}{m_s} & 0\\ 0 & 0 & \frac{1}{I_i} & -\frac{1}{I_i} & 0 & 0 & -\frac{R_i}{I_i}\end{bmatrix}\begin{bmatrix}x_e\\ \dot{x}_e\\ p_1\\ p_2\\ x_s\\ \dot{x}_s\\ q_i\end{bmatrix}+\begin{bmatrix}0 & 0\\ \frac{1}{M_e} & \frac{G_s}{M_e}\\ 0 & 0\\ 0 & 0\\ 0 & 0\\ 0 & \frac{-G_s}{m_s}\\ 0 & 0\end{bmatrix}\begin{bmatrix}F_e\\ i_s\end{bmatrix} \tag{4.21}$$

The output of this dynamical system is a vector of the transmitted force and mount displacement $\boldsymbol{Y}=[F_T\ \ x_e\ \ \dot{x}_e\ \ p_1\ \ p_2\ \ x_s\ \ \dot{x}_s\ \ q_i]^T$.

$$\begin{bmatrix}F_T\\ x_e\\ \dot{x}_e\\ p_1\\ p_2\\ x_s\\ \dot{x}_s\\ q_i\end{bmatrix}=\begin{bmatrix}K_r & B_r & -A_r & 0 & k_s & b_s & 0\\ 1 & 0 & 0 & 0 & 0 & 0 & 0\\ 0 & 1 & 0 & 0 & 0 & 0 & 0\\ 0 & 0 & 1 & 0 & 0 & 0 & 0\\ 0 & 0 & 0 & 1 & 0 & 0 & 0\\ 0 & 0 & 0 & 0 & 1 & 0 & 0\\ 0 & 0 & 0 & 0 & 0 & 1 & 0\\ 0 & 0 & 0 & 0 & 0 & 0 & 1\end{bmatrix}\begin{bmatrix}x_e\\ \dot{x}_e\\ p_1\\ p_2\\ x_s\\ \dot{x}_s\\ q_i\end{bmatrix}+\begin{bmatrix}0 & G_s\\ 0 & 0\\ 0 & 0\\ 0 & 0\\ 0 & 0\\ 0 & 0\\ 0 & 0\end{bmatrix}\begin{bmatrix}F_e\\ i_s\end{bmatrix} \tag{4.22}$$

We can easily see the effect of the inputs (current and engine force) on the individual states of the system (pressures, transmitted force, flow rate, etc.). In the previous system of equations, the engine force and the current are the inputs of the system (engine disturbances is considered as an input along with the control current).

4.3 Simulations and Analysis

Simulations with the Laplace Domain Transfer Functions

We validated our passive hydraulic engine mount model in Chapter 2 and validated the model of solenoid in Chapter 3. In previous Section 4.1 and 4.2 the model of our active engine mount is developed. In this section, we will study the effect of different terms in the model of active engine mount through simulating the relations that has been developed in Section 4.1.

Solenoid parameters (the active component of the mount as introduced in section 4.1) are given in Table 4-1. These parameters along with the parameters from Table 2-1 will be used throughout this Chapter.

Table 4-1: The parameters of the active component of the model.

Parameter	Name	Value	Unit
Pumping area of solenoid plunger	A_s	2.897×10^3	mm^2
Mass of plunger	m_s	0.261	Kg
Stiffness of plunger	k_s	5.9	$\frac{N}{mm}$
Damping of plunger	b_s	0.03	$\frac{N.s}{mm}$

Two terms contribute to the transmitted force equation in (4.16): (1) the displacement of the engine, and (2) the current fed to actuator. Separating the passive hydraulic component of force transmission and the active component of force transmission, we obtain two coefficients as (4.32) and (4.24).

$$\overline{C_{F_T X_e}} = \left[K_r + B_r s + A_r^2 \Psi + \frac{(k_s + b_s s)(A_s A_r \Psi) - A_s^2 A_r^2 \Psi^2}{m_s s^2 + b_s s + (k_s + A_s^2 \Psi)} \right], \tag{4.23}$$

which is the transmitted force due to engine displacement. As we expect in Equation (4.23) only passive and mass, damping and stiffness of the plunger can be seen. The effect of displacements of the solenoid is not directly seen in this equation. Moreover the term of interaction of mass, stiffness and damping (the last term in (4.23)) is much smaller than the first three terms of stiffness, damping and hydraulic pressure and therefore it is negligible.

Equation (4.24) is the transmitted force coefficient due to the solenoid actuation:

$$\overline{C_{F_T I_s}} = \left[G_s + G_s \frac{A_r A_s \Psi - (k_s + b_s s)}{m_s s^2 + b_s s + (k_s + A_s^2 \Psi)} \right], \tag{4.24}$$

which shows the effect of the actuated solenoid on the transmitted force to the chassis.

In Equation (4.24), the first term G_s, is the direct contribution of solenoid's internal force. The second term is the interaction of the plunger motion with the stiffness and damping of the solenoid and the plunger with the fluid pressure. Examining Equation (4.24), we expect to see that at higher frequencies the coefficient reduces to G_s, as the other term vanishes. So increasing the solenoid gain directly increases the system capability to change the transmitted force. At higher frequencies, the plunger mass does not respond to the forces applied to it, so it does not move much. Therefore, the displacement and velocity of the plunger decrease, and in that case, the effect of damping and stiffness of the plunger seen in equation (4.3) is minimal. Figure 4-3 shows the frequency response of the whole term along in (4.24) with the solenoid gain. Dashed line is the simple model where the force on the chassis is modelled by the internal attraction of

the coil-plunger, whereas the solid line is with the full model, which considers interaction of the fluid, mass, acceleration, damping, and stiffness of the plunger.

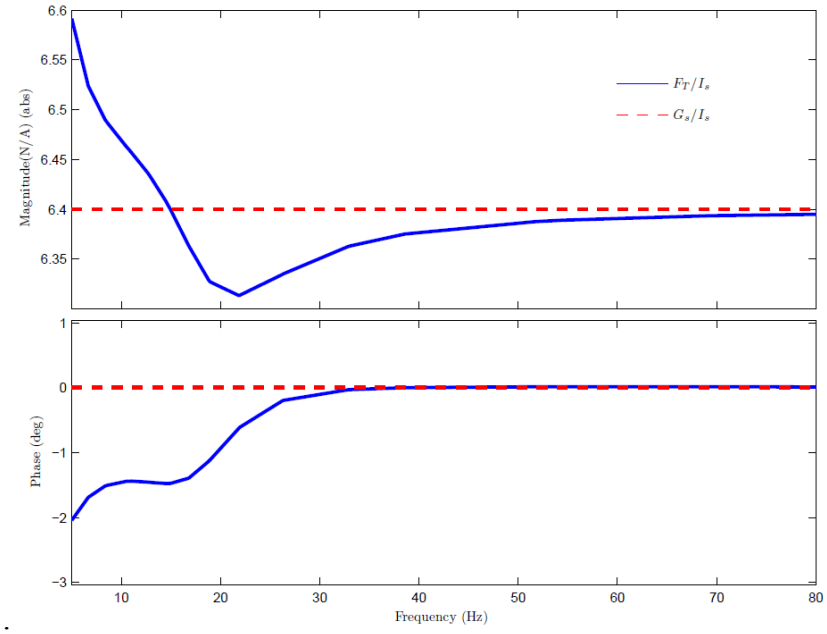

Figure 4-3: Force applied to chassis by actuating the solenoid.

Next, we study whether or not a change in the plunger mass affects the applied force to the chassis. Figure 4-4 is the simulation of transmitted force for different plunger masses, a graph comparing the generated force by -50%, -20%, +20% and +100% of the mass of plunger. An improvement in force generation is seen at low frequencies (5-10 Hz) by decreasing the mass of plunger, and a decrease in the force is observed at higher frequencies; the changes however are not substantial.

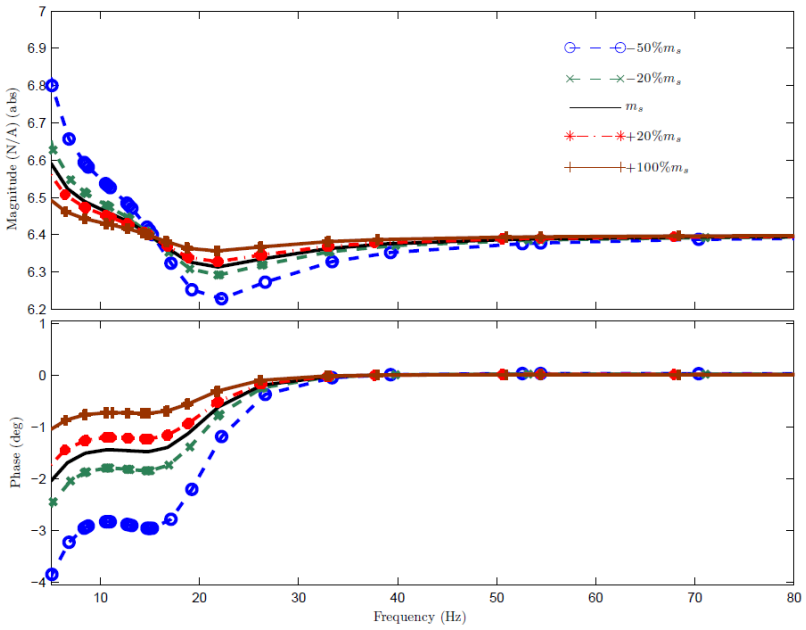

Figure 4-4: Effect of the changing the mass of plunger during change in the applied force to the chassis.

Figure 4-5 shows the effect of changing the stiffness of the solenoid in the transmitted force to the chassis. Again, increasing the stiffness of the plunger increases the transmitted force at low frequency, but it does not affect the force at high frequency.

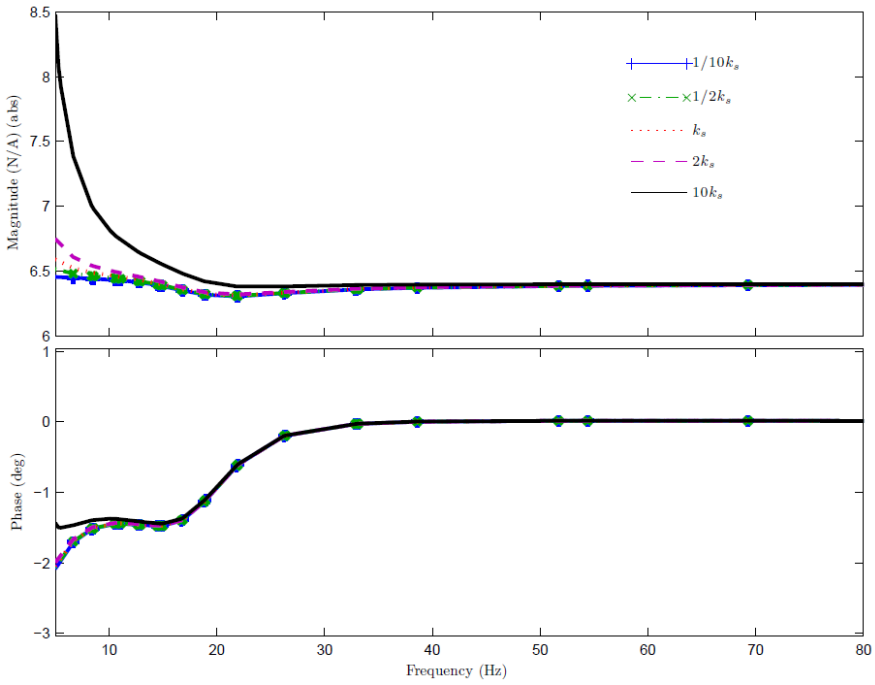

Figure 4-5: Effect of changing the stiffness of the solenoid, in the force applied to the chassis.

Taking a look back at (4.3) we see that the pressure of pumping chamber is an important factor in the transmitted force to the chassis. Therefore we need to see the effect of solenoid motion on the pressure of the pumping chamber. From Equation (4.15) we can see that the contribution of the pressure force on the transmitted force is:

$$P_1 A_r = -\left[\frac{G_s A_r A_s \Psi}{m_s s^2 + b_s s + (k_s + A_s^2 \Psi)}\right] I_s. \tag{4.25}$$

The frequency response of the pressure force transmitted in response to the control current I_s is shown in Figure 4-6. This graph shows that the force generated by the pressure is negligible in contrast to the internal force of the solenoid (compare with Figure 4-3).

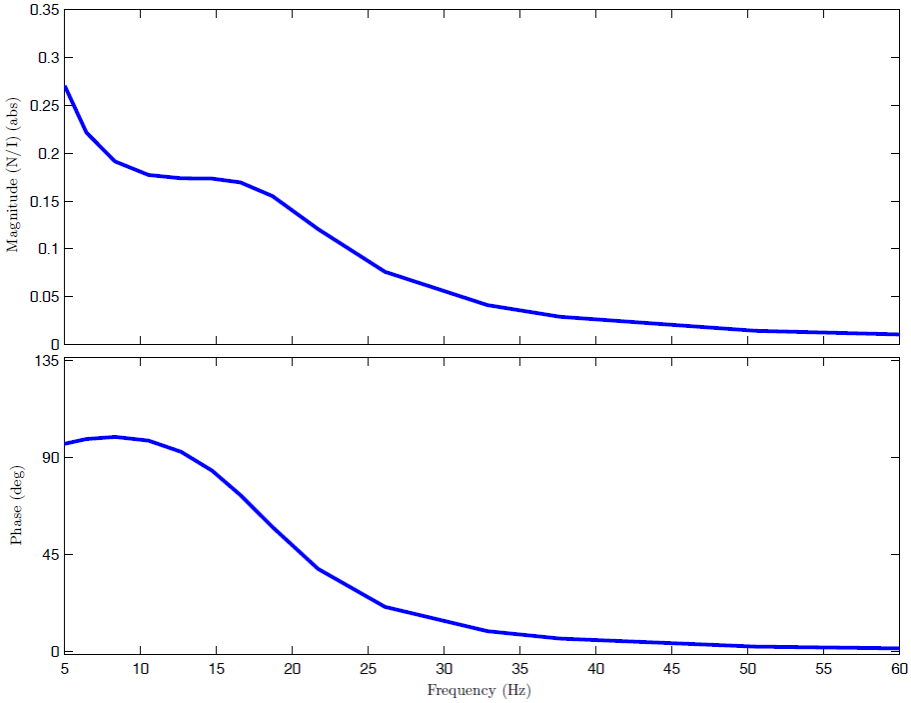

Figure 4-6: Pressure force transmitted to the chassis due to actuating the solenoid.

Tuning the Dynamic Stiffness of the Active Engine Mount

The dynamic stiffness of an active engine mount must tuneable. The tuning must enhance the noise and vibration condition of the chassis. As discussed before, in each driving condition a certain stiffness and damping is desirable. Therefore let assume that the dynamic stiffness of the passive hydraulic mount that we tested in Chapter 2 must be tuned. In Chapter 3 an actuator was added to the hydraulic mount but the mount has the same passive elements (same rubber, same inertia track, same geometry).

In Equation (4.18) the dynamic stiffness of the active engine mount is given. We can see that the dynamic stiffness of the active mount is a function of the I_s/X_e. I_s/X_e is an actuation function in feed-forward or feedback control scheme where the current I_s is commanded to the solenoid coil based on a displacement sensor readings, X_e. By changing this function, the

dynamic stiffness of the active mount changes (See Figure 4-7). In Chapter 2, the dynamic stiffness of a passive mount was given (rewritten as (4.26)).

$$K_{dyn}\big|_{pass.} = [K_r + B_r s + \frac{A_r^2}{C_1}\frac{I_i s^2 + R_i s + \frac{1}{C_2}}{I_i s^2 + R_i s + \frac{1}{C_1} + \frac{1}{C_2}}]. \tag{4.26}$$

Let us also call the dynamic stiffness of the active mount

$$\begin{aligned} K_{dyn}\big|_{act.} = &\Big[K_r + B_r s + A_r^2\Psi \\ &+ \frac{(k_s + b_s s)(A_s A_r \Psi) - A_s^2 A_r^2 \Psi^2}{m_s s^2 + b_s s + (k_s + A_s^2\Psi)}\Big] \\ &+ G_s\left[1 + \frac{A_r A_s \Psi - (k_s + b_s s)}{m_s s^2 + b_s s + (k_s + A_s^2\Psi)}\right]\frac{I_s}{X_e}. \end{aligned} \tag{4.27}$$

Here if we design a proper actuation function we can modify the active mount's dynamic stiffness to a portion or a multiple of the passive engine mount, so that

$$\zeta_k K_{dyn}\big|_{pass.} = K_{dyn}\big|_{act.}, \tag{4.28}$$

where ζ_k is a coefficient of stiffness tuning.

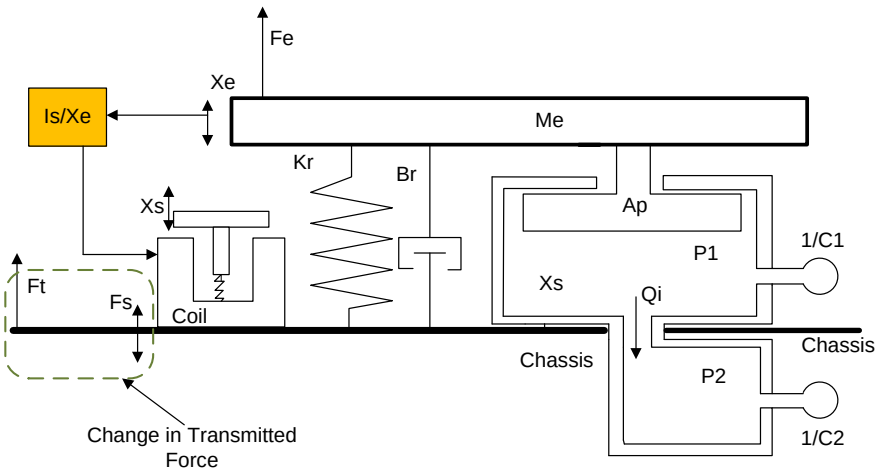

Figure 4-7: Dynamic Stiffness Tuning.

Based on our modelling, we set the coefficient of stiffness tuning to 0.2, 0.5, 0.7, 1, 1.5 and 2. Where coefficients lower than 1 result in softer mount and coefficient bigger than 1 generates harder mount and the coefficient equal to 1 is the same as passive hydraulic mount. The tuned dynamic stiffness is given in Figure 4-8. To see what type of actuation function is required to accomplish these tunings. As we expected, the change in stiffness does not affect the phase shift of the mount. Figure 4-10 shows the response of the actuation function I_s/X_e, used to soften or harden the mount. For example, to soften the mount to $0.7K_d$ at 20 (Hz) and for an engine displacement of 0.1 (mm), a sinusoidal current approximately equal to 1 (A) with 180 phase shift is required.

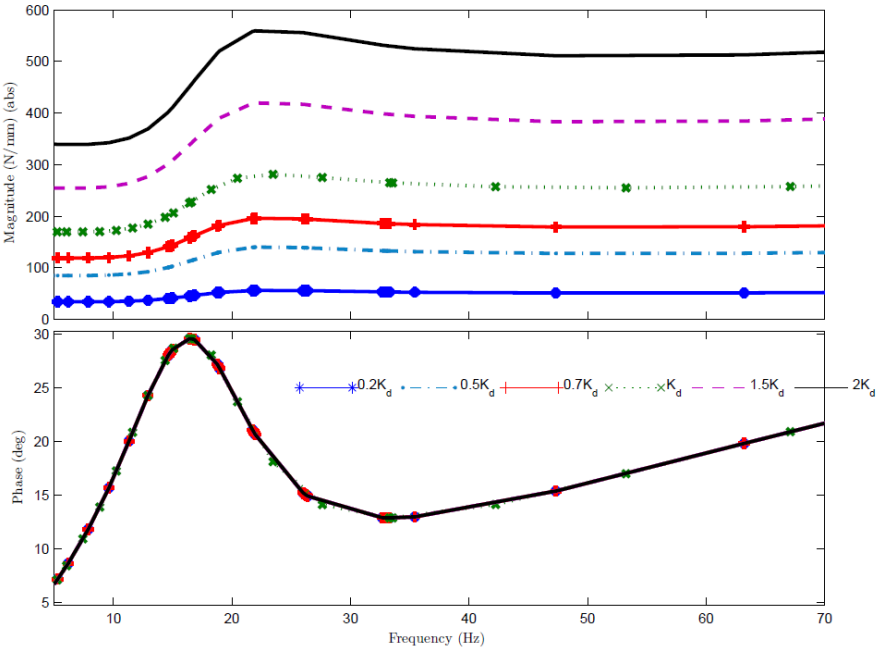

Figure 4-8: The tuned stiffness of active hydraulic mount.

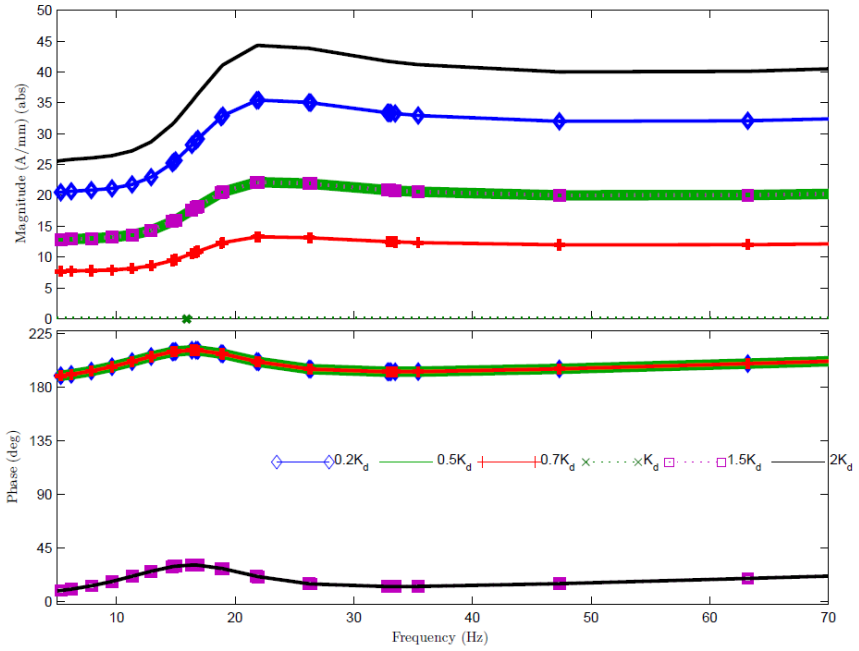

Figure 4-9: The applied transfer function for increasing or decreasing the mount stiffness.

Controlling the Transmissibility

The force transmission coefficient or transmissibility, $T_r = \frac{F_T}{F_e}$, is a factor shows how much force is transmitted to the chassis. Figure 4-10 is the transmissibility of the passive hydraulic engine mount. As expected, the phase is negative because the system is causal, and the phase is close to -180 because the transmitted force is a direct result of engine displacements which itself is in 180 degrees phase shift from the engine forces (Engine force and engine displacement are in 180 degree shift as acceleration and displacement of an oscillatory motion is (see 4.2)).

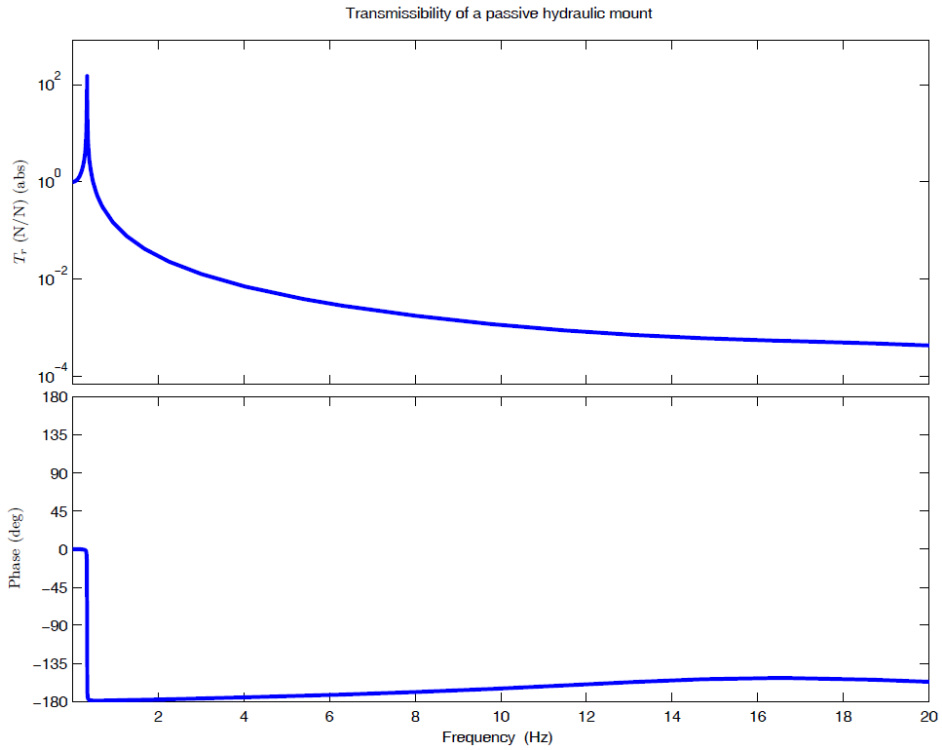

Figure 4-10: Transmissibility of the hydraulic engine mount.

The transmissibility of an active engine mount can be tuned also. The transmissibility change mechanism is shown in Figure 4-11.

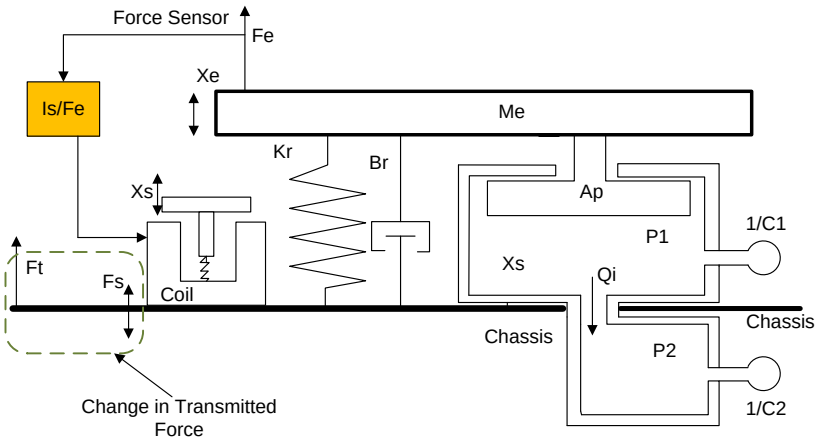

Figure 4-11: Transmissibility tuning scheme.

Because we assumed that the system is linear, therefore the superposition quality of linear systems holds here, therefore we can say that the transmitted force is the summation of the engine force transmission of the passive system and the solenoid force transmission to the chassis.

$$F_T|_{tot} = F_T|_{eng} + F_T|_{sol}, \tag{4.29}$$

where $F_T|_{tot}$ is the total transmitted force, $F_T|_{eng}$is the transmitted force due to engine displacement only, and $F_T|_{sol}$ is the transmitted force due to solenoid actuation only. At each engine condition an specific engine unbalance force, F_e, is generated. Dividing the both sides of (4.29) we get

$$T_{r_{act}} = \frac{F_T|_{tot}}{F_e} = \frac{F_T|_{eng}}{F_e} + \frac{F_T|_{sol}}{F_e}, \tag{4.30}$$

where $T_{r_{act}}$ is the transmissibility of the active engine mount. The first term in the right hand side of (4.30), $T_{r_{pass}} = \frac{F_T|_{eng}}{F_e}$, is the passive transmissibility that has been defined before and simulated in Figure 4-10. Here we write the second term in (4.30) as

$$\frac{F_T|_{sol}}{F_e} = \frac{F_T}{I_s}(I_s/F_e), \tag{4.31}$$

where F_T/I_s is the dynamics of force generation of the solenoid and its transmission to the chassis (the model of the physical system) and (I_s/F_e) is the transfer function between a sensed engine unbalance force into a control current. Therefore with proper design of (I_s/F_e), we can control the transmissibility. Here we introduce $\zeta_{T_r} = T_{r_{act}}/T_{r_{pass}}$ as a coefficient of transmissibility reduction where $\left(\zeta_{T_r} - 1\right) * 100$ is the percentage of transmissibility reduction. For example a $\zeta_{T_r} = 1/2$, means 50% transmissibility reduction.

$$T_{r_{act}} = \zeta_{T_r} T_{r_{pass}} = T_{r_{pass}} + \frac{F_T}{I_s}\,(I_s/F_e), \tag{4.32}$$

Figure 4-12 shows the frequency response of transfer functions required to reduce the transmissibility by 30, 50, 80, and 100%. Notice that 100% reduction of transmissibility means full vibration disturbance cancellation on the chassis.

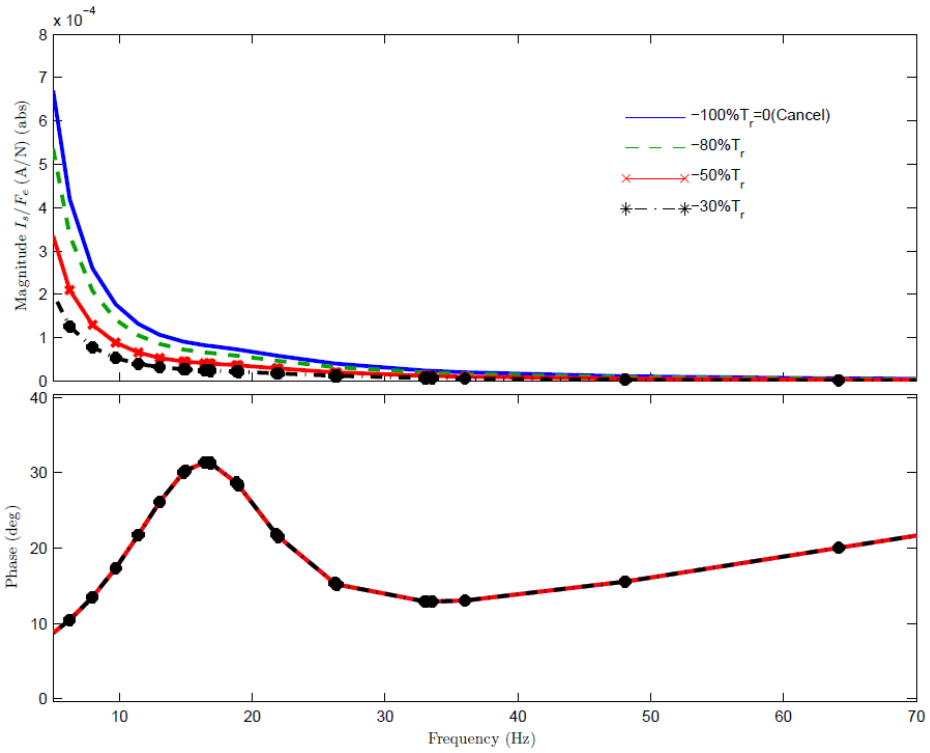

Figure 4-12: $\frac{I_S}{F_e}$ function for modifying the transmissibility of the mount.

4.4 Experimental Verification of the Active Mount Force Output

To verify the effect of the identified solenoid on the force transmitted to the chassis, we built a rigid frame to fix the two ends of the mount. The frame has a mechanical jack to preload the engine mount. A force sensor is attached to the tip of the mount. This way, we measure the applied force to the chassis while sweeping the current input over a frequency range (see Figure 4-13).

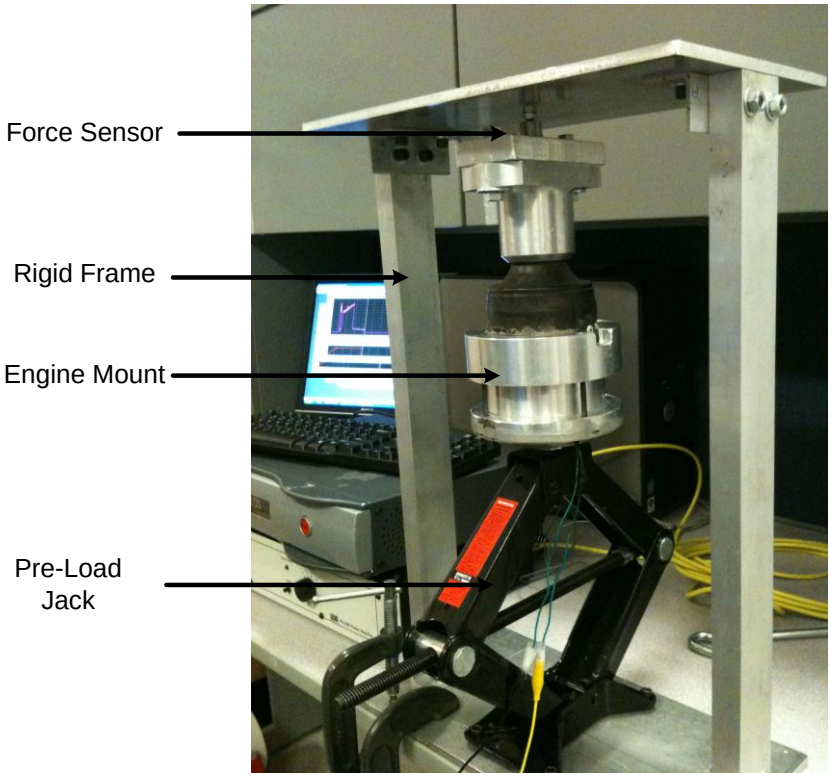

Figure 4-13: Test-bed to measure the force of solenoid actuation applied to the chassis.

The results of the frequency sweep are presented in Figure 4-14. The force response has white noise, which we think is due to problems with the signal conditioning of the load cell. However, the trend and value of the response are very close to what we expect from theory.

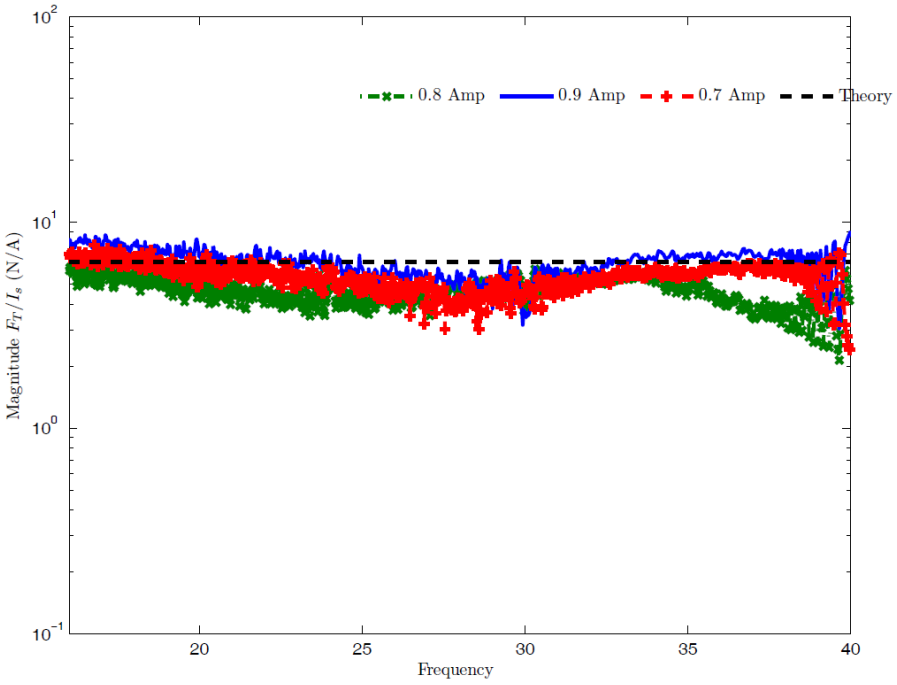

Figure 4-14: Normalised results of three tests compared with the simplified expected transmitted force.

In another test, we applied a transfer function for the solenoid input current as

$$\frac{0.3s^2 + 4s + 5000}{0.3s^2 + 4s + 5200}. \tag{4.33}$$

The bias current in this test was 1 (A), and a sinusoidal function with 0.8 (A) was passed through the previous transfer function. The normalized result of this experiment is shown in Figure 4-15.

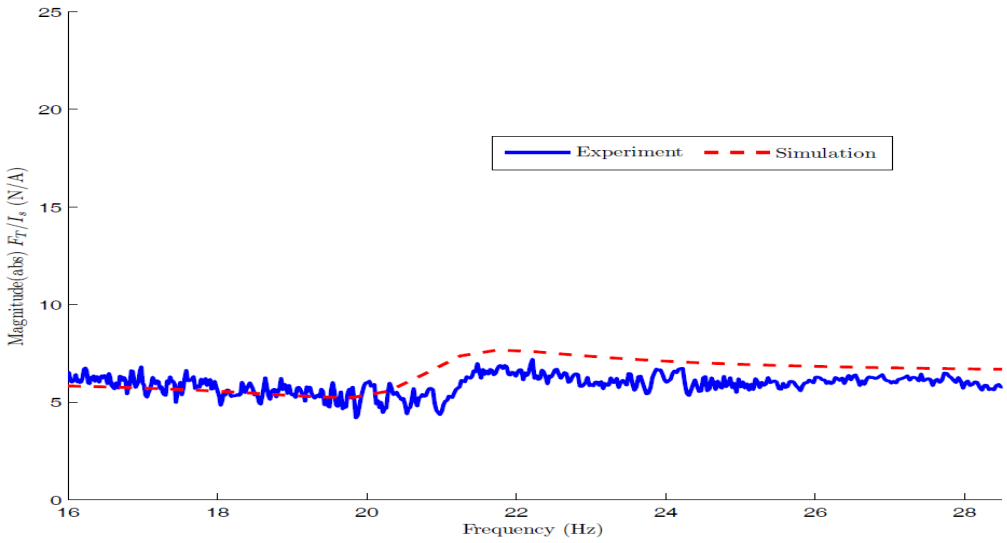

Figure 4-15: Transmitted force of active engine mount (Theory vs. Experiment).

In another test the previous transfer function in (4.33) is replaced with the following transfer function,

$$\frac{0.13s^2 + 2s + 5000}{0.13s^2 + 2s + 5200}, \tag{4.34}$$

and the results are show in and compared with the expected value.

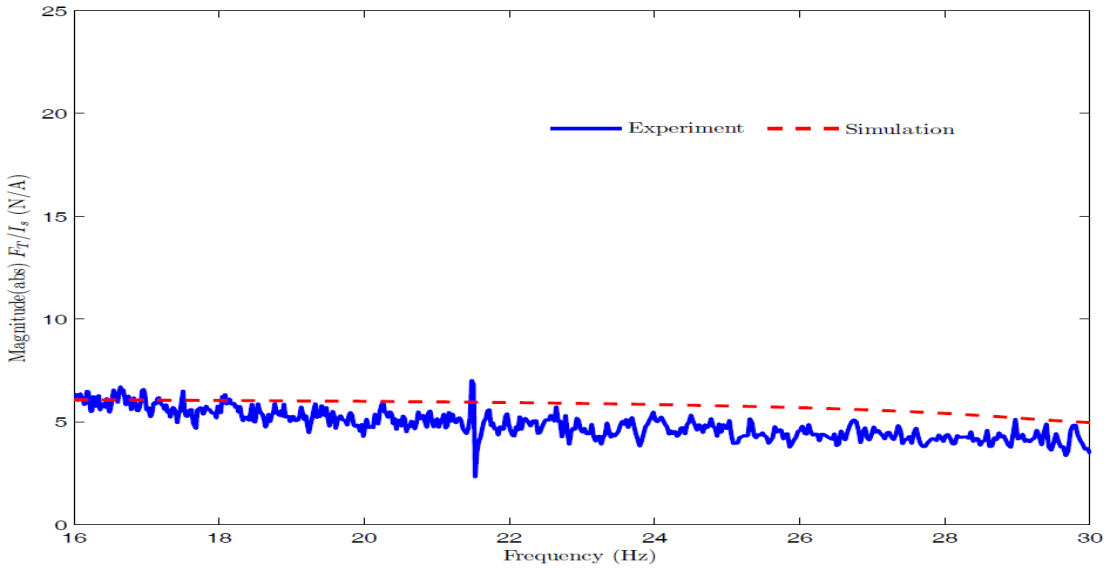

Figure 4-16: The force response of the active engine mount (Theory vs. Experiment).

The response is given in Figure 4-16 and it is compared with the ideal response. Again, we see that the response is approximately following the theoretical expectation. Therefore, the active part of the derived linear model of engine mount is verified because the simulations of the model agree with the experimental results.

4.5 Active Dynamic Stiffness Tuning Experiment

The same experimental test bed used in Chapter 2 (Figure 2-6) for testing the dynamic stiffness of the hydraulic engine mount is used in this section to test the active engine mount. Actuating the solenoid generates a force that can alter the transmitted force and the dynamic stiffness of the mount. Here the active engine mount is tested with a control transfer function given in equation (4.35).

$$\frac{I_s}{X_e} = \frac{(s+90)^2}{s(s+240)} \,. \tag{4.35}$$

By plugging in the previous equation into equation (4.18), the mathematical model of the dynamic stiffness is obtained. The active engine mount is tested in higher frequencies (35-60 Hz) and the result of deploying this active transfer function in comparison to a passive mode hydraulic mount is shown in Figure 4-17. It also shows that the obtained mathematical model is predicting the change in the dynamic stiffness. As you can see in Figure 4-17, the model closely predicts the stiffness and damping of the mount. The actuator effort in this feed-forward control function is between 0.4 to 0.6 (A), which is in the operating range of the solenoid actuator. This mount tuning can be used for cruising at steady-state in high gear and satisfies.

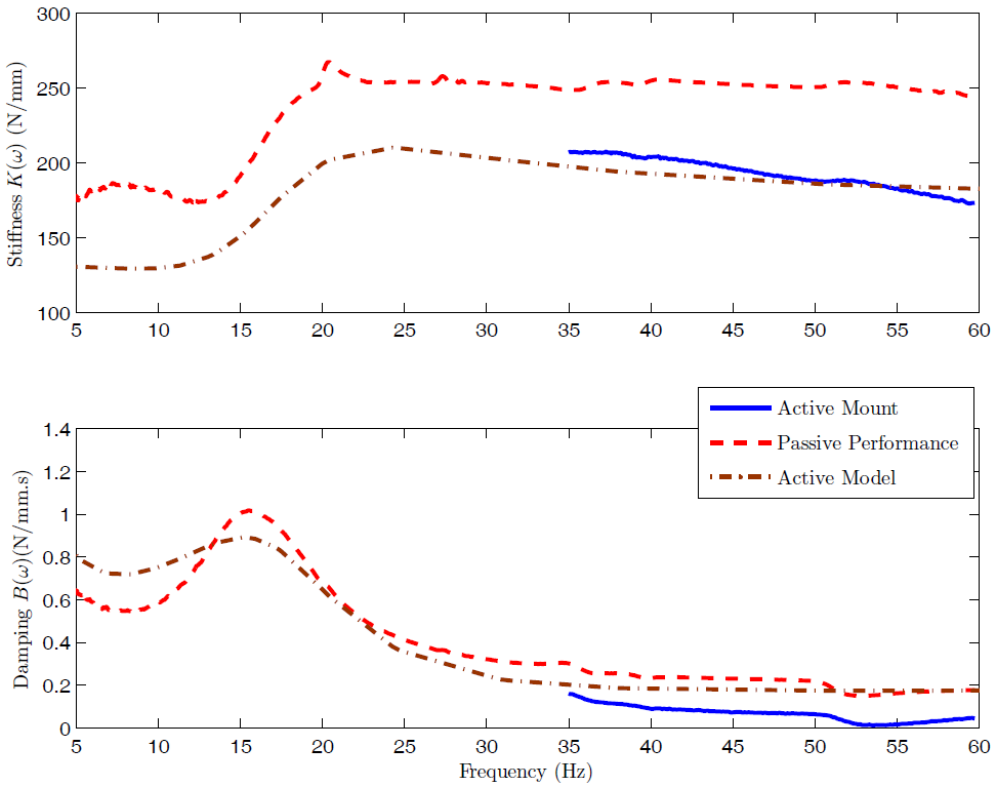

Figure 4-17: Stiffness and damping of the hydraulic mount in passive mode (dashed line), stiffness and damping of the active mount in a soft mode (solid line), and stiffness and damping based on the derived model and the function used in experiment (graphs 0.1 mm peak-peak engine displacement)

The transfer function (4.35) satisfies the engine mount requirement number 4 given in Figure 2-15. This shows that we were able to analytically model the solenoid-based active hydraulic engine mount. By properly designing the active control transfer functions this engine mount is capable of changing its dynamic stiffness to desirable levels.

A control theory study for design and comparing different active vibration control strategies based on the model that has been developed in this thesis can be the next step in this research.

Chapter 5: CONCLUSION AND FUTURE WORK

5.1 Conclusion

The design, identification, modelling, simulation and verification of an active hydraulic engine mount were studied in this thesis. We showed that a solenoid can be used as a cost-efficient yet effective alternative to the more expensive actuators that are being used in design of active mounts. We demonstrated that in our application the highly nonlinear model of the solenoid can be estimated by a linear equation. The internal force between plunger and coil is directly related to the current flowing in the coil. Superposing the linear model of solenoid actuator and the developed linear model of the passive hydraulic mount, we came up with a linear model for the active solenoid-based hydraulic engine mount.

For simplicity, we can say that the coil is attached to the chassis. The force to the chassis is in phase with the applied current. By sensing the relative displacement of the engine, we studied the design feasibility of a feed-forward controller for changing the dynamic stiffness of the mount. Moreover, in simulations, we examined the feed-forward path requirements for changing the transmissibility of the mount. To verify the model, a rigid frame was built to fix the two ends of the mount and pre-load it. The force output of the mount agrees closely with our expectations from the simulation. Finally through dynamic stiffness tuning tests, we showed that the developed governing equation of the active mount can closely predict the behaviour of the system, therefore it is reliable and can be used in control design analysis and sizing of the similar active engine mounts.

5.2 Future Direction

Following are the recommended future directions of this research:

- Modelling the solenoid as a multiple piecewise linear device and coupling those models with the system equations of the engine mount.
- Performing the force transmissibility tests and implementing the proposed transfer functions for changing the force transmissibility.
- Studying the different closed-loop control methods of active engine isolation so as to deal with the uncertainty in the model as well as the inputs – that is, robust control, stochastic control, loop-shaping, sliding mode, intelligent control.
- Using soft computing methods for modelling/controlling the actuator and/or the engine mount.
- Sizing the solenoid actuator based on the engine mount isolation requirements.
- Coupling the force model of a conventional engine with the engine mount model.
- Further study of the feasibility of replacing the solenoid with other actuator technologies such as piezoelectric, pneumatic, hydraulic, and electrostatic.
- Studying the possibility of using force sensor, and accelerometer, instead of position sensor and examining the effect on the precision and cost of the control system.
- Designing the electronics and software required for communication of the active engine mount with the ECU of a car.
- Implementing it on a vehicle and performing road tests.

APPENDICES

Appendix A: Solenoid Data Sheet

MAGNETIC SENSOR SYSTEMS

Tubular Low Profile Clapper Solenoid

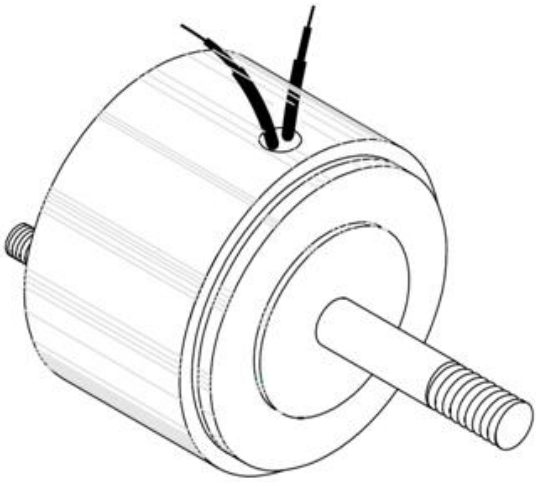

Series S-16-264

2 5/8" DIA X 1.56"
[66.8 mm X 39.6 mm]

TOTAL WEIGHT: 34.7 OUNCES [984 GR]
PLUNGER WEIGHT: 9.3 OUNCES [264 GR]

duty cycle maximum "ON" time, (Sec.)	1 ∞	1/2 230	1/4 90	1/10 30
watts approximate ampere turns	20 1200	40 1700	80 2400	200 3800

AWG number	resistance (Ω)	volts DC	volts DC	volts DC	volts DC
19	1.4	5.2	7.3	10.3	16.3
20	1.8	5.8	8.2	11.5	18.2
21	3.0	7.7	10.9	15.3	24.3
22	4.5	9.6	13.6	19.2	30.5
23	7.8	12.1	17.2	24.2	38.3
24	12.0	15.5	21.9	31.0	49.0
25	18.5	19.1	27.1	38.3	60.6
26	32.5	25.1	35.5	50.2	79.4
27	48.4	31.4	44.5	62.8	99.4
28	75.2	39.6	56.1	79.2	125
29	127	50.9	72.1	102	161
30	201	63.4	89.9	127	201
31	313	78.3	111	157	248
32	469	97.6	138	195	309
33	770	124	176	249	393
34	1330	161	228	321	509
35	2257	207	293	413	654

HEAT SINK: For proper heat dissipation, body of solenoid should be mounted on an equivalent of 5.0" x 5.0" x 1/4" aluminum plate in an unrestricted flow of air.

6901 Woodley Avenue, Van Nuys, California 91406
Telephone: (818) 785-6244 Fax: (818) 785-5713
www.solenoidcity.com

S-16-264 MECHANICAL DIMENSIONS

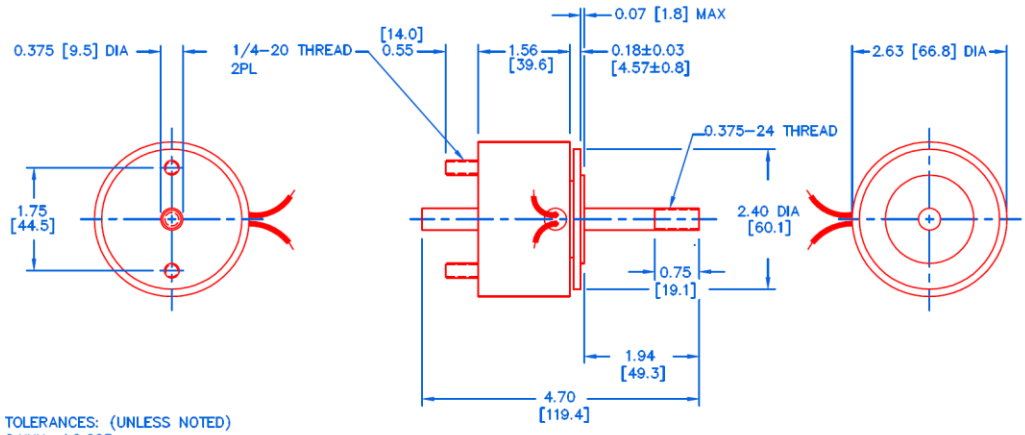

TOLERANCES: (UNLESS NOTED)
0.XXX: ±0.005
0.XX : ±0.010
X/X: ±1/64
COIL RESISTANCE: ±10%
DIMENSIONS IN INCHES [mm]

SOLENOID SHOWN ENERGIZED

TYPICAL PULL FORCE VERSUS STROKE

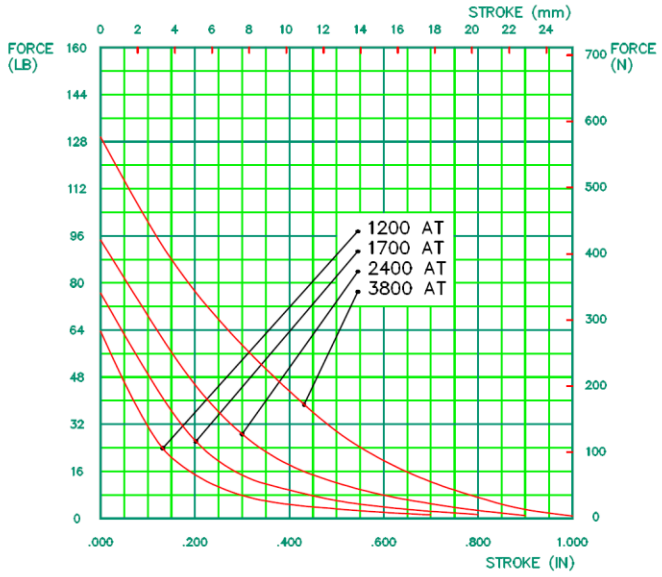

WORKS CITED

[1] J.E. Colgate, C.T. Chang, Y.C. Chiou, W.K. Liu, and L.M. Keer, "Modelling of a hydraulic engine mount focusing on response to sinusoidal and composite excitations," *Journal of Sound and Vibration*, vol. 184, pp. 503 - 528, 1995.

[2] Daniel J. Inman, *Engineering Vibration*, 3rd ed.: Prentice Hall, 2008.

[3] Rajendra Singh and Song He, "Anatomy of a Real-Life Non-Linear Device: Hydraulic Engine Mount," in *XXV International Modal Analysis Conference*, Orlando, FL, 2007.

[4] T Ushijima, K Takano, and H Kojima, "High Performance Hydraulic Mount for Improving Vehicle Noise and Vibration," *SAE Paper # 880073*.

[5] R. Singh, G. Kim, and P.V. Ravindra, "Linear analysis of automotive hydro-mechanical mount with emphasis on decoupler characteristics," *Journal of Sound and Vibration*, vol. 158, pp. 219 - 243, 1992.

[6] Aaron Geisberger, Amir Khajepour, and Farid Golnaraghi, "Non-linear modelling of hydraulic mounts: theory and experiment," *Journal of Sound and Vibration*, vol. 249, pp. 371 - 397, 2002.

[7] Aaron Geisberger, Hydraulic Engine Mount Modeling, Parameter Identification and Experimental Validation, 2000, M.Sc. Thesis University of Waterloo.

[8] A.R. Ohadi and G. Maghsoodi, "Simulation of Engine Vibration on Nonlinear Hydraulic Engine Mounts," *Trans. of ASME, Journal of Vibration and Acoustics*, vol. 129, pp. 417-424, 2007.

[9] S.B. Choi, Y.T. Choi, C.C. Cheong, and Y.S. Jeon, "Performance Evaluation of a Mixed Mode ER Engine Mount Via Hardware-in-the-Loop Simulation," *Journal of Intelligent Material Systems and Structures*, vol. 10, pp. 671-677, 1999.

[10] Seung-Bok Choi and Young-Tai Choi, "Sliding mode control of a shear-mode type ER engine mount," *Journal of Mechanical Science and Technology*, vol. 13, pp. 26-33, 1999.

[11] Mehdi Ahmadian and Young Kong Ahn, "Performance Analysis of Magneto-Rheological Mounts," *Journal of Intelligent Material Systems and Structures*, vol. 10, pp. 248-256, 1999.

[12] G. Kim and R. Singh, "A study of passive and adaptive hydraulic engine mount systems with emphasis on non-linear characteristics," *Journal of Sound and Vibration*, vol. 179, no. 427-453, 1995.

[13] Mahmoud S. Foumani, Amir Khajepour, and Mohammad Durali, "A New High-Performance Adaptive Engine Mount," *Journal of Vibration and Control*, vol. 10, pp. 39-45, 2004.

[14] P.M.T Fursdon, A.J. Harrison, and D.P. Stoten, "The design and developement of a self-tuning active engine mount," in *IMechE2000 Conference Transaction*, 2000, pp. 21-32.

[15] Takao Ushijima and Syoichi Kumakawa, "Active Engine Mount with Piezo-Actuator for Vibration Control," SAE, 930201 1993.

[16] D.A. Hodgson, "Frequency-Shaped Control of Active Isolators," in *AHS and Royal Aeronautical Society, Technical Specialists' Meeting on Rotorcraft Acoustics/Fluid Dynamics*, Philadelphia, PA, 1991.

[17] Rahman A. Shoureshi and Thomas Knureck, "Automotive applications of a hybrid active noise and vibration control," *Control Systems Magazine, IEEE* , vol. 16, no. 6, pp. 72-78, Dec 1996.

[18] H. Hartwig, M. Haase, and H.-J. Karkosch, "Electromagnetic actuators for active engine vibration cancellation," in *7th international conference on new actuators ACTUATOR 2000*, Bremen, 2000.

[19] S. Elliott, I. Stothers, and P. Nelson, "A multiple error LMS algorithm and its application to the active control of sound and vibration," *Acoustics, Speech and Signal Processing, IEEE Transactions on*, vol. 35, pp. 1423-1434, 1987.

[20] A.J. Hillis, A.J.L Harrison, and D.P. Stoten, "A comparison of two adaptive algorithms for the control of active engine mounts," *Journal of Sound and Vibration*, vol. 268, pp. 37-54, 2005.

[21] A.J. Hillis, S.A. Neild, D.P. Stoten, and A.J.L Harrison, "A minimal controller synthesis algorithm for narrow-band applications.," in *Proceedings of the Institution of Mechanical Engineers -- Part I -- Journal of Systems & Control*, 2005, pp. 591-607.

[22] Continental AG. (Accessed Octobre 2010) http://www.contitech.de/pages/produkte/schwingungstechnik/motorlagerung/aktive_tilger_en.html.

[23] C. Bohn, A. Cortabarria, V. Haertel, and K. Kowalczyk, "Active control of engine-induced vibrations in automotive vehicles using disturbance observer gain scheduling," *Control Engineering Practice*, vol. 12, pp. 1029-1039, September 2004.

[24] DTR VMS. (Accessed Octobre 2010) http://www.dtrvms.com/pt_ham.asp.

[25] Sergey E. Lyshevski, *Electromechanical Systems, Electric Machines, and Applied Mechatronics*.: CRC, 1999.

[26] A. Ghaffaria, F. Najafia M. Taghizadeha, "Modeling and identification of a solenoid valve for PWM control applications," *C. R. Mecanique 337*, 2009.

[27] Yunhe Yu, Saravanan M. Peelamedu, Nagi G. Naganathan, and Rao V. Dukkipati, "Automotive Vehicle Engine Mounting Systems: A Survey," *Journal of Dynamic Systems, Measurement, and Control*, vol. 123, pp. 186-194, 2001.

[28] G. Nakhaie Jazar and M.Farid Golnaraghi, "Nonlinear Modeling, Experimental Verification, and Theoretical Analysis of a Hydraulic Engine Mount," *Journal of Vibration and Control*, vol. 8, pp. 87-116, 2002.

[29] A.Masih Hosseini, Hossein Mansour, Siamak Arzanpour, M.Farid Golnaraghi, and M.Ash Parameswaran, Design of Active and Semi-Active Hydraulic Engine Mounts, 2010, AUTO21 HQP Conference, Theme F, 7 - 11 July 2010, Windsor, Ontario, Canada.

[30] D.A. Swanson, "Active engine mounts for vehicles," in *International OFF-highway and Powerplant Congress & Exposition, SAE Technical Paper Series 932432*, Milwaukee, Wisconsin, 1993.

[31] Hossein Mansour, Design and Developement of Active and Semi-Active Engine Mount, 2010, M.A.Sc. Thesis, Simon Fraser University.

[32] Hossein Mansour, Siamak Arzanpour, and Farid Golnaraghi, "Active Decoupler Design for Hydraulic Engine Mount With Application in Variable Displacement Engines," *Journal of Vibration and Control*, vol. In Press.

[33] R. Singh, "Dynamic design of automotive systems: Engine mounts and structural joints," *Sadhana*, vol. 25, pp. 319-330, 2000.

[34] (Accessed Novembre 2010) Cooper Standard. [Online]. http://www.cooperstandard.com/powertrain_mounts.php